EXCLUSIVE RARE B DECAYS

Study of $B \to K\ell^+\ell^-$ and $B \to K^*\ell^+\ell^-$ decays in the Standard Model and Supergravity models

TROELS C. PETERSEN PETER ZEILER SKANDS

24/01/2000

NIELS BOHR INSTITUTE
Department for Experimental High Energy Physics

Project concluding the B physics study group at NBIHEP in the fall of 1999.

FOR THE EVALUATION:

- Sections 2, 3, 6, and 7 are mainly the work of Peter Z. Skands
- Sections 4 and 5 are mainly the work of Troels C. Petersen
- The introduction and conclusion have been written jointly.
- Appendix A is the work of Troels C. Petersen
- Appendix B is the work of Peter Z. Skands

Supervisor:
Prof. Alexander Khodjamirian
Niels Bohr Institute, HEP
Blegdamsvej 17, Copenhagen Ø
khodjam@nbi.dk

Troels C. Petersen
190675 – 2057

Peter Z. Skands
151177 – 2547

Contents

List of Figures

List of Tables

1 Introduction

The subject of B-physics, taking its name from the B mesons and b quarks studied, has been gaining interest during the last decade over which the possibilities for experimental study in this field have increased dramatically. Especially the subject of rare B decays has come into focus lately, as Flavour Changing Neutral Current (FCNC) b-quark transitions provide important testing grounds for the Standard Model (SM), the rates and distributions of these decays being sensitive to possible higher mass scales and/or new interactions.

This sensitivity stems from the fact that FCNC processes originate from loop diagrams[1] dominated by virtual heavy particles (t, W, Z), and thus there is more room for new physics to appear e.g. by replacing the loop particles with supersymmetric ones and/or including interactions not found in the SM. These points will be discussed more closely below. There is also the possibility of determining entries in the CKM mixing matrix with greater precision, yet as is also indicated by the title, the important issue here is that of determining the effects of the supersymmetric supergravity models on observable quantities and comparing these with the predictions of the SM. Making the subject of B physics all the more interesting is the fact that these decays, although rare, will soon come under experimental scrutiny at high-statistics experiments at detectors such as BaBar, Belle, HERA-B, CDF and in the future ATLAS, CMS and LHC-B.

1.1 The project outline

Following the most recent theoretical studies of the $B \to K^{(*)}\ell^+\ell^-$ decay, we have gone through the derivation of the hadronic matrix element, done the calculation of the decay width and reproduced the numerical results, with [1] as a reference. Furthermore, we have used the allowed ranges of short distance coefficients in supersymmetric supergravity to calculate signatures of such models.

In section 2 we go through the free quark decay and see why the FCNC are suppressed relative to tree-level processes. Section 3 establishes the effective operators for the $B \to K^{(*)}\ell^+\ell^-$ decay, from which we construct an effective Hamiltonian at the scale m_b using the Renormalization Group method. We then in section 4 write down the matrix element, which after the inclusion of long distance effects and the introduction of form factors, is fully hadronic. From this we go through the calculation of the decay distribution in detail in section 5, and we also calculate the forward-backward asymmetry, a quantity well suited for minimizing both theoretical as well as experimental errors. We then present a rather brief introduction to supersymmetry in section 6 and discuss the $B \to K^{(*)}\ell^+\ell^-$ decay in the light of supergravity models. After these theoretical discussions follows the numerical calculations in section 7, and finally we give some concluding remarks.

2 Decays of free quarks

As an introduction, we shall consider the somewhat unphysical scenario of free quark decay. This means that we shall ignore, for the time being, the complexities due to QCD interactions of the quarks and the hadronic structure of the B and K mesons. This approximation will gradually be removed in the following sections. It is also understood that we here work in the context of the standard model.

[1] i.e. they are of higher order in the electroweak couplings, hence the name *rare* transitions.

2.1 FCNC transitions

For both of the decays $B \to K\ell^+\ell^-$ and $B \to K^*\ell^+\ell^-$ the corresponding quark transition is $b \to s\ell^+\ell^-$. Thus, for the free quark decay amplitude, this is what we need to consider. It is obvious that the quark flavour changes and that the electric charge does not, hence the name Flavour Changing Neutral Current (FCNC).

In the SM, only the $W^\pm$ couple to flavour changing vertices, and so only flavour changing *charged* current processes exist at the one-vertex level (fig.1a)[2].

$$\begin{aligned} d_i &= (d, s, b) \\ u_j &= (u, c, t) \\ q_i &= (u, d, s, c, b, t) \end{aligned}$$

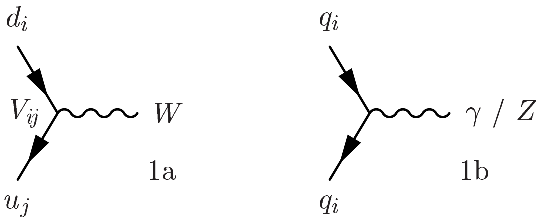

Figure 1: Elementary electroweak quark vertices in the SM. A factor of V_{ij} reflecting the degree of mixing in the CKM matrix is associated with the vertex in fig.1a. No change of quark flavour occurs in fig.1b.

Thus, we need to construct more complicated diagrams to obtain FCNC transitions. To lowest order (smallest number of electroweak vertices and no gluons), we need to combine no less than four elementary vertices, yielding the diagrams in fig.2.

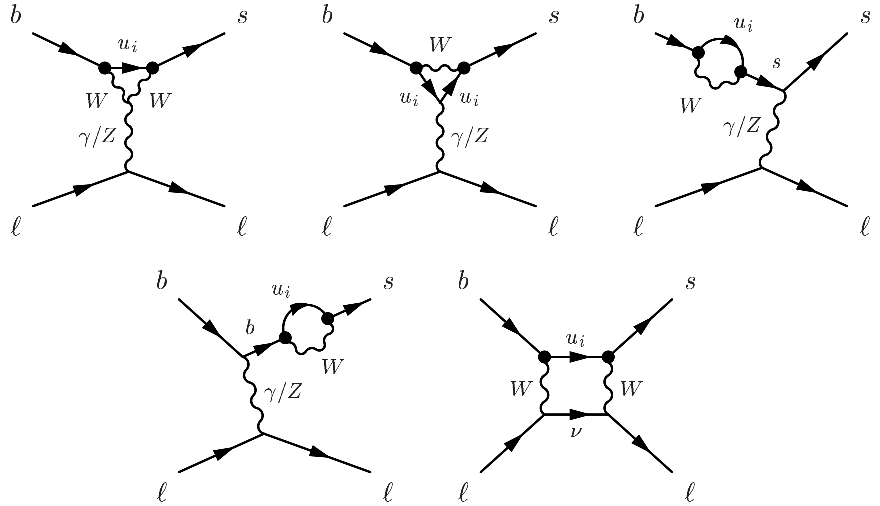

Figure 2: Lowest order FCNC $b \to s\ell^+\ell^-$ transitions in the SM. Dots denote flavour changing vertices with V_{CKM} factors, and $u_i = (u, c, t)$. The two first diagrams are known as penguins [3], the two next can be called penguin mutants (necessary to make the penguin diagrams gauge invariant by attaching the γ/Z to all possible lines.), and the last is, for obvious reasons, called a box diagram.

[2] The fact that flavour-changing neutral currents are suppressed is supported by experimentally observed low branching ratios for $B \to X_s\gamma$ decays [2] ($b \to s\gamma$ at the quark level). One may also mention the non-observation of $Z \to b\bar{s}$ decays at the same level as $Z \to b\bar{b}, s\bar{s}$.

2.2 GIM cancellation

In addition to the loop structure of the FCNC diagrams, there is a mechanism which causes them to be further suppressed. This mechanism, which owes to the unitarity of the CKM matrix[3], is known as GIM cancellation (Glashow-Illiopoulos-Maiani) and we shall now describe briefly how it works:

The diagrams in fig.2 contain a sum over the virtual u, c, and t-quark contributions multiplied by their respective V_{CKM} entries: V_{qb} from $b \to q$ multiplied by V_{qs}^* from $q \to s$. This is general for all FCNC transitions, making the following arguments valid not only for the decay being considered here, but for all FCNC transitions in the Standard Model:

$$\mathcal{M}(b \to s\ell^+\ell^-) = V_{ub}V_{us}^*\mathcal{M}_u + V_{cb}V_{cs}^*\mathcal{M}_c + V_{tb}V_{ts}^*\mathcal{M}_t \tag{1}$$

In this sum, the matrix elements will in general be different, however if $m_u = m_c = m_t$, then $\mathcal{M}_u = \mathcal{M}_c = \mathcal{M}_t = \tilde{\mathcal{M}}$, and we would have:

$$\mathcal{M}(b \to s\ell^+\ell^-) = \tilde{\mathcal{M}} \sum_{q=u,c,t} V_{qb}V_{qs}^* \tag{2}$$

From unitarity of the CKM matrix, the sum in eq. (2) must vanish (sum over q):

$$V_{qb}V_{qs}^* = V_{q3}V_{q2}^* = V_{q3}V_{2q}^\dagger = \left(V^\dagger V\right)_{23} = \delta_{23} = 0 \tag{3}$$

Thus, all contributions cancel and the matrix element vanishes. This is the essence of GIM cancellation. However, in reality the quark masses are not equal, and so GIM cancellation cannot completely rid the world of FCNC processes; it merely *suppresses* them.

To further determine the properties of the matrix elements, we make use of the so-called *light quark rearrangement*. Assuming unitarity of the CKM matrix for three generations of quarks, we can write:

$$\begin{aligned}
\mathcal{M}\left(b \to s\ell^+\ell^-\right) &= V_{ub}V_{us}^*\mathcal{M}_u + V_{cb}V_{cs}^*\mathcal{M}_c + V_{tb}V_{ts}^*\mathcal{M}_t \\
&= -(V_{cb}V_{cs}^* + V_{tb}V_{ts}^*)\mathcal{M}_u + V_{cb}V_{cs}^*\mathcal{M}_c + V_{tb}V_{ts}^*\mathcal{M}_t \\
&= V_{cb}V_{cs}^*(\mathcal{M}_c - \mathcal{M}_u) + V_{tb}V_{ts}^*(\mathcal{M}_t - \mathcal{M}_u) \\
&\equiv V_{cb}V_{cs}^*\overline{\mathcal{M}_c} + V_{tb}V_{ts}^*\overline{\mathcal{M}_t}
\end{aligned} \tag{4}$$

We see immediately that any quark-mass independent terms will cancel in the $\overline{\mathcal{M}}_{c,t}$ and so the answer will be proportional to powers of m_c and m_t. Since $m_t \gg m_c$, the t-quark part will dominate.

3 Effective Hamiltonian

Now we have the elementary diagrams which we need for calculating the free quark amplitudes to lowest order. At some point, however, we must to turn on QCD, preferably while keeping the interaction, $\mathcal{H}$, expressed in as simple a form as possible. To this end, an *effective* Hamiltonian is constructed replacing the full theory by an effective point interaction; a process divided into two main steps:

[3] We shall assume unitarity of the CKM matrix for three generations of quarks. This unitarity is supported experimentally [4].

1. Integrating out the internal parts of the diagrams in fig.2 (propagators of Z, W, t), leaving only operators corresponding to the external light particles in the resulting Hamiltonian (section 3.1). As the electroweak coupling is small at all relevant scales, it is sufficient for our purposes to work in lowest order with respect to electroweak interactions.

2. Including short-distance QCD corrections, i.e. gluon exchanges between the quark lines (section 3.2). Including long-distance QCD effects is a more complicated procedure, due to the non-perturbative nature of QCD at long distances. This will be treated when the matrix element is constructed in section 4.

3.1 Four-fermion operators

3.1.1 Effective FCNC vertices

In calculating the FCNC diagrams in fig.2 directly, one constructs an effective lowest order weak Hamiltonian, $\mathcal{H}_w^0$, containing only operators corresponding to external light particles. Knowing the Feynman rules for the elementary vertices and propagators, one can integrate out the loops of the heavy W, Z, t, thus obtaining a set of "effective Feynman rules" for the vertices in fig.3 which are still of the lowest order in the electroweak couplings and which contain no QCD corrections (see e.g. [5]).

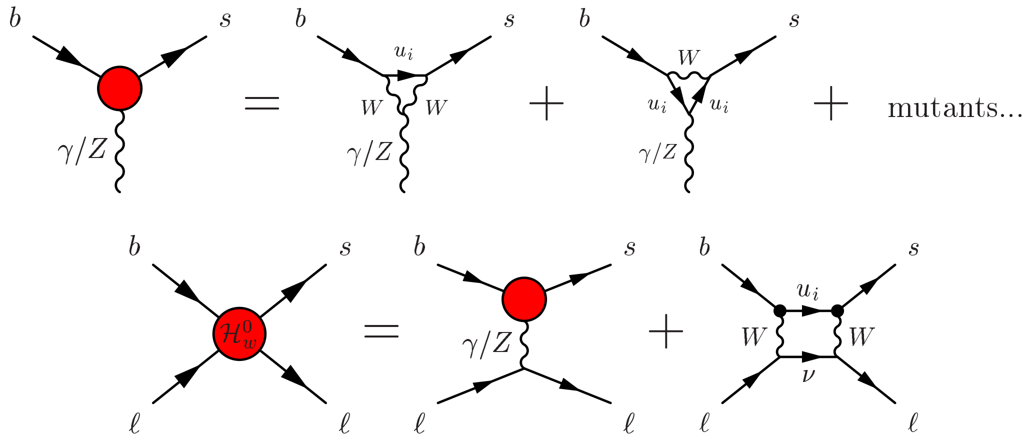

Figure 3: Upper: Effective penguin vertex resolved in terms of the contributing diagrams. Lower: Effective four-fermion $b \to s\ell^+\ell^-$ vertex resolved in terms of penguin and box contributions. ($u_i = (u, c, t)$)

The effective vertices depend on the masses of the internal particles, and consequently they can be calculated as functions of

$$x_i = \frac{m_i^2}{m_W^2}, \qquad i = u, c, t \tag{5}$$

Note that, as mentioned in the discussion of GIM cancellation (section 2.2), we usually only need to take x_t into account[4].

[4] Some complication due to the c quark does occur due to $c\bar{c}$ resonant intermediate states, however these will be discussed when the matrix element is constructed (see section 4.2).

3.1.2 Operator Product Expansion (OPE)

As there is only a limited number of possibilities for FCNC effective vertices, a set of universal functions can be found describing all FCNC processes (Inami and Lim [6]). The total Hamiltonian (in the absence of QCD) then becomes a sum over local four-fermion operators each multiplied by some coefficient depending on x_t:

$$\boxed{\mathcal{H}_w^0 = \frac{G_F}{\sqrt{2}} V_{tb} V_{ts}^* \sum_k C_k(x_t) \mathcal{O}_k}$$

The C_k are called Wilson coefficients and contain the internal short-distance physics (apart from the V_{CKM} factors and G_F) whereas the effective operators, $\mathcal{O}_k$, contain the external quark and lepton operators corresponding to the initial and final states (see below). Note that all the $C_k(x_t)$ are known in terms of the universal functions, owing to the calculability of the effective vertices. With this formulation, we have obtained a compact, calculable form of the electroweak Hamiltonian. This approach, embodied in the above equation, is known as the Operator Product Expansion (OPE) [5].

Now we are interested in the detailed forms of the effective operators, $\mathcal{O}_k$. Having integrated out the internal particles and put their physics in the Wilson coefficients, not much is left but to specify how the colour flows and what the chiral structure of the interaction is. The colour flow must be specified as colour is a conserved quantum number in QCD and as diagrams with different colour flow give rise to different contributions. In $b \to s\ell^+\ell^-$ decays, with only two of the external lines being quarks, there is only one way to let the colour flow, and only two operators contribute directly at the electroweak scale, namely $\mathcal{O}_{9V}$ and $\mathcal{O}_{10A}$ ([5]), which are respectively the vector and axial components of the diagrams in fig.2. $\mathcal{O}_{9V}$ and $\mathcal{O}_{10A}$ are therefore dubbed semi-leptonic operators.

In addition to these, $\mathcal{O}_{7\gamma}$ also contributes; $\mathcal{O}_{7\gamma}$ is a $b \to s\gamma$ operator having a tensor structure ($\bar{b}\sigma_{\mu\nu} s F^{\mu\nu}$) which contributes to $b \to s\ell^+\ell^-$ through $\gamma \to \ell^+\ell^-$. A list of operators entering FCNC calculations[5] (and of which we shall need quite a few when evolving to lower energy scales) is given in table 1.

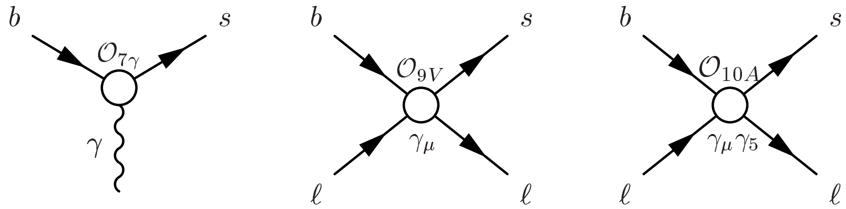

Figure 4: The effective operators $\mathcal{O}_{7\gamma}$, $\mathcal{O}_{9V}$, and $\mathcal{O}_{10A}$ relevant to semileptonic decays.

3.2 Short distance QCD effects

In order to make realistic calculations, one has to include quark-gluon interactions, adding the elementary quark-gluon vertices to our set of effective Feynman rules.

At momentum scales larger than $\approx$ 1GeV, α_s is smaller than 0.5. At the electroweak scale we have $\alpha_s(m_Z) \approx 0.118$ [4], and so we are in a position to use perturbation theory for calculating the effects of gluon exchanges between the quarks. However, even within perturbation theory, the

[5]There are additional operators not shown, e.g. for the $b \to d$ transitions and non-leptonic modes.

$$\textbf{Current-Current}\left\{\begin{array}{lcl}\mathcal{O}_1 & = & (\bar{s}_\alpha c^\beta)_{V-A}(\bar{c}_\beta b^\alpha)_{V-A}\\ \mathcal{O}_2 & = & (\bar{s}_\alpha c^\alpha)_{V-A}(\bar{c}_\beta b^\beta)_{V-A}\end{array}\right.$$

$$\textbf{QCD penguins}\left\{\begin{array}{lcl}\mathcal{O}_3 & = & (\bar{s}_\alpha b^\alpha)_{V-A}\sum_{q=u,d,s,c,b}(\bar{q}_\beta q^\beta)_{V-A}\\ \mathcal{O}_4 & = & (\bar{s}_\alpha b^\beta)_{V-A}\sum_{q=u,d,s,c,b}(\bar{q}_\beta q^\alpha)_{V-A}\\ \mathcal{O}_5 & = & (\bar{s}_\alpha b^\alpha)_{V-A}\sum_{q=u,d,s,c,b}(\bar{q}_\beta q^\beta)_{V+A}\\ \mathcal{O}_6 & = & (\bar{s}_\alpha b^\beta)_{V-A}\sum_{q=u,d,s,c,b}(\bar{q}_\beta q^\alpha)_{V+A}\end{array}\right.$$

$$\textbf{Electroweak penguins}\left\{\begin{array}{lcl}\mathcal{O}_7 & = & \frac{3}{2}(\bar{s}_\alpha b^\alpha)_{V-A}\sum_{q=u,d,s,c,b}\left(e_q(\bar{q}_\beta q^\beta)_{V+A}\right)\\ \mathcal{O}_8 & = & \frac{3}{2}(\bar{s}_\alpha b^\beta)_{V-A}\sum_{q=u,d,s,c,b}\left(e_q(\bar{q}_\beta q^\alpha)_{V+A}\right)\\ \mathcal{O}_9 & = & \frac{3}{2}(\bar{s}_\alpha b^\alpha)_{V-A}\sum_{q=u,d,s,c,b}\left(e_q(\bar{q}_\beta q^\beta)_{V-A}\right)\\ \mathcal{O}_{10} & = & \frac{3}{2}(\bar{s}_\alpha b^\beta)_{V-A}\sum_{q=u,d,s,c,b}\left(e_q(\bar{q}_\beta q^\alpha)_{V-A}\right)\end{array}\right.$$

$$\textbf{Magnetic Penguins}\left\{\begin{array}{lcl}\mathcal{O}_{7\gamma} & = & \frac{e}{8\pi^2}m_b\bar{s}_\alpha\sigma^{\mu\nu}(1+\gamma_5)b^\alpha F_{\mu\nu}\\ \mathcal{O}_{8G} & = & \frac{g}{8\pi^2}m_b\bar{s}_\alpha\sigma^{\mu\nu}(1+\gamma_5)T^a_{\alpha\beta}b^\beta G^a_{\mu\nu}\end{array}\right.$$

$$\textbf{Semi-leptonic}\left\{\begin{array}{lcl}\mathcal{O}^\ell_{9V} & = & (\bar{s}_\alpha b^\alpha)_{V-A}(\bar{\ell}\ell)_V\\ \mathcal{O}^\ell_{10A} & = & (\bar{s}_\alpha b^\alpha)_{V-A}(\bar{\ell}\ell)_A\end{array}\right.$$

Table 1: The effective operators relevant to $b \to s\ell^+\ell^-$ transitions [5]. α and β are colur indices to be summed over, emphasizing the colour flow inherent in the operators. Note that $\mathcal{O}_{7\gamma}$, $\mathcal{O}_{9V}$, and $\mathcal{O}_{10A}$ only have one colour index, reflecting that there is only one possible colour flow. The subscripts $V \pm A$ refer to chiral structure, thus $(\bar{q}q)_{V\pm A} = (\bar{q}\gamma_\mu(1\pm\gamma_5)q)$. The current-current operators $\mathcal{O}_{1,2}$ are due to tree-level W-exchange between the quark currents, and $\mathcal{O}_{3-6}$ are due to penguin diagrams similar to fig.2 where instead of γ/Z one has gluon exchange and instead of a lepton pair one has a quark pair with flavour $q = (u, d, s, c, b)$. $\mathcal{O}_{7-10}$ are due to penguin diagrams similar to fig.2, but where the lepton pair is interchanged with a quark pair. $\mathcal{O}_{8G}$ is similar to $\mathcal{O}_{7\gamma}$, but with a gluon instead of a photon.

calculations quickly become complicated due to the multitude of diagrams arising even to first order (see fig.5 opposite).

To begin the truly formidable task of calculating all of these diagrams as well as the ones of higher order is, however, not necessary. One of the principal advantages of the OPE approach is that having integrated out the heavy degrees of freedom, we merely need to include gluon corrections to the $\mathcal{O}_i$. This greatly simplifies the calculations and is illustrated in fig.6.

3.2.1 Renormalization Group

As we have seen, we are able to calculate the Wilson coefficients at momentum scales, $\mu = m_W$. However, the momenta involved in B decays are typically of the order of $m_b \ll m_W$, and so we need some method of evolving the result to lower scales. One of the problems facing us is that the diagrams in fig.6 contain corrections of order $\alpha_s \ln(m_W/\mu)$ which are negligible at $\mu = m_W$, but which clearly become important at $\mu \ll m_W$ due to the growth of the logarithms. At n loops, these corrections will appear to the n^{th} power, and thus we need some method for resumming them.

A very reliable and elegant way of summing up the $(\alpha_s \ln(m_W/\mu))^n$ corrections is known as the

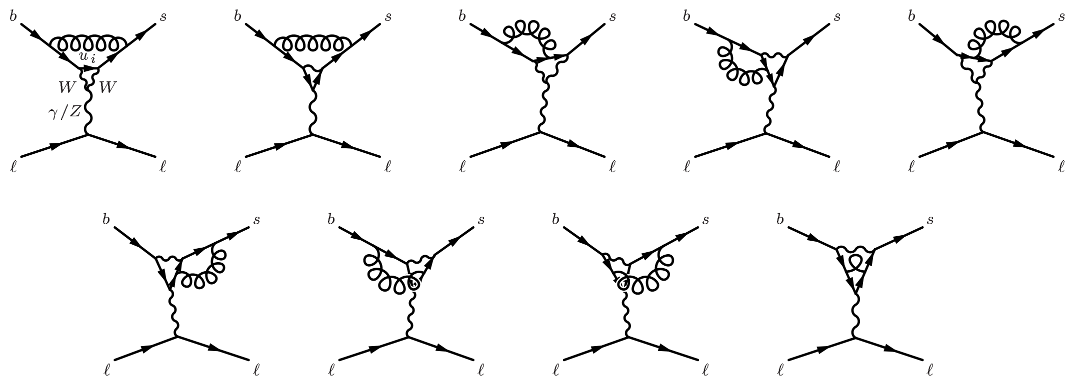

Figure 5: Some of the first order gluon corrections to the penguin diagrams, the gluons being symblized by the curly lines. The diagrams not shown can be constructed by attaching the gluon twice to the same quark line. Similar diagrams must be constructed for the box diagrams as well as diagrams of higher order.

Gluon corrections to $\mathcal{O}_{7\gamma}$ and $\mathcal{O}_{9V}$ introducing operator mixings.

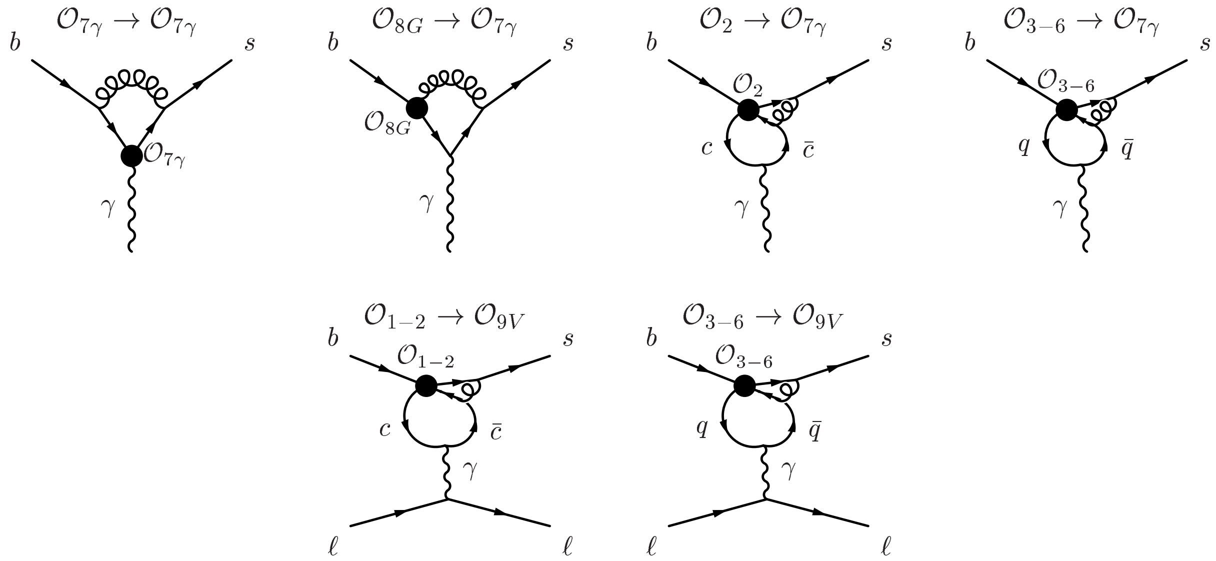

Figure 6: First order gluon corrections to the effective operators $\mathcal{O}_i$ generating mixings with $\mathcal{O}_{7\gamma}$ and $\mathcal{O}_{9V}$. These corrections contain $\alpha_s \ln(m_W/\mu)$ contributions which become large when going to scales lower than m_W. Although finite order of α_s corrections will also arise, these can be contained in the Wilson coefficients. Note that the axial vector operator $\mathcal{O}_{10A}$ is not mixed with other $\mathcal{O}_i$ due to parity conservation. The additional diagrams required for gauge invariance have not been shown.

Renormalization Group method [7]. The result of this summation is cast as a matrix equation:

$$C_i(\mu) = \sum_j U_{ij}(\mu, m_W) C_j(m_W) \tag{6}$$

where U, the evolution matrix, is obtained from known quantities by integration over γ_{ij}, the matrix of anomalous dimension (see [8]). The non-diagonal structure of γ_{ij} causing mixings between different effective operators can be seen from fig.6.

Although scale dependence will enter both in the Wilson coefficients and in the $\mathcal{O}_i$, the resulting

Hamiltonian should still be scale independent, as the physically observable matrix element cannot depend on the theoretician's choice of renormalization scale.

3.2.2 Result for effective Hamiltonian

Having integrated out the internal physics in the OPE approach and evolved the C_i and the $\mathcal{O}_i$ to the scale m_b by the Renormalization Group method, the effective Hamiltonian acquires the following form[6]:

$$\mathcal{H}_{\text{eff}} = -4\frac{G_F}{\sqrt{2}} V_{tb} V_{ts}^* \sum_i C_i(\mu) \mathcal{O}_i(\mu) \tag{7}$$

where the $C_i(m_b)$ have been calculated in the theoretical literature with rather high precision. A detailed description of this calculation is beyond our project. For numerical applications, we use the values of C_i presented in [1]:

C_1	C_2	C_3	C_4	C_5	C_6	C_7^{eff}	C_9	C_{10}
-0.248	+1.107	+0.011	-0.026	+0.007	-0.031	-0.313	+4.344	-4.669

Table 2: Standard Model Wilson coefficients at the scale $\mu = m_b$. $C_7^{\text{eff}} = C_7 + C_5/3 - C_6$ (see section 4.1).

4 The matrix element

Now we turn to the matrix element for the $B \to K^{(*)}\ell^+\ell^-$ decays. We have an effective Hamiltonian, which puts us in a position to formally write down the *quark level* matrix element at scales down to m_b. Long distance effects, i.e. effects down to the scale of Λ_{QCD} such as four-quark operator contributions and resonances, also need to be included. The final step towards a *hadronic* matrix element, is to include form factors, which parameterizes hadronic dynamics.

4.1 Quark level matrix element.

Formally, the quark level matrix element for the decay $b \to s\ell^+\ell^-$ is defined as follows:

$$\mathcal{M}(b \to s\ell^+\ell^-) \equiv < s\ell^+\ell^- | \mathcal{H}_{\text{eff}} | b >, \tag{8}$$

with the effective Hamiltonian eq.(7) and the $\mathcal{O}_i$ and their corresponding coefficients given in table 1 and 2 respectively.

In addition to $\mathcal{O}_{9V}$ and $\mathcal{O}_{10A}$, which contribute directly (figure 7a) and $\mathcal{O}_{7\gamma}$, which contributes through $\gamma \to \ell^+\ell^-$ (figure 7b), the amplitude of $b \to s\ell^+\ell-$ also gets contributions from the four-quark operators $\mathcal{O}_i, i = 1, ..., 6$ by the subsequent transitions $b \to sq\bar{q}$, $q\bar{q} \to \gamma \to \ell^+\ell^-$ (figure 7c). In first approximation, the propagation of intermediate quarks can be calculated in pertubation theory as a loop diagram yielding an effective quark-lepton operator, which mainly has a vector structure. Therefore this contribution can be included in a simple manner by redefining the $\mathcal{O}_{9V}$

[6] This is the conventional form used in the rare decay literature, see [7, p.503].

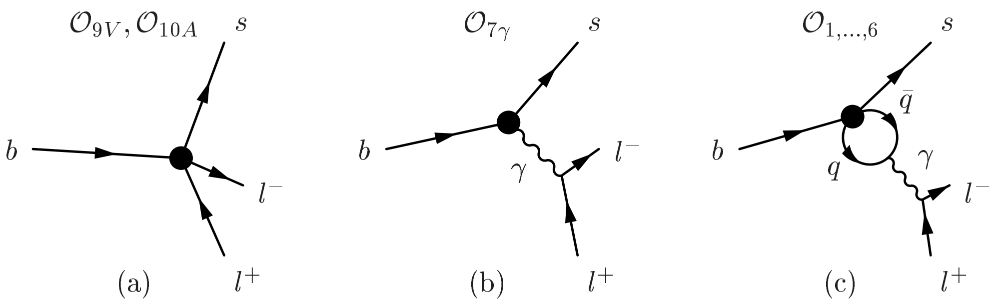

Figure 7: Diagrammatical representation of the operators $\mathcal{O}_i$. (a) shows the semi-leptonic operators, (b) shows the electromagnetic operator and (c) shows the four-quark operators, which contribute through $q\bar{q} \to \gamma \to \ell^+\ell^-$.

Wilson coefficient C_9, and one obtains:

$$\begin{aligned} C_9^{\text{eff}}(s) &= C_9 + Y_{pert}(s), &(9)\\ Y_{pert}(s) &\equiv g(m_c, s)(3C_1 + C_2 + 3C_3 + C_4 + 3C_5 + C_6) - \frac{1}{2} g(m_b, s)(4C_3 + 4C_4 + 3C_5 + C_6) - \\ &\quad \frac{1}{2} g(0, s)(C_3 + 3C_4) + \frac{2}{9}(3C_3 + C_4 + 3C_5 + C_6), &(10) \end{aligned}$$

where the Wilson coefficients to leading logarithmic order are listed in table 2, and the loop functions g (with $m_{u,d,s}$ taken to be zero) are [5]:

$$\begin{aligned} g(m, s) &= -\tfrac{8}{9}\ln\tfrac{m}{\mu} + \tfrac{8}{27} + \tfrac{4}{9}x - \tfrac{2}{9}(2+x)\sqrt{|1-x|}\left\{ \begin{array}{ll} \ln\left|\frac{\sqrt{1-x}+1}{\sqrt{1-x}-1}\right| - i\pi, & \text{for } x \equiv 4m^2/s < 1 \\ 2\arctan\left(\frac{1}{\sqrt{x-1}}\right), & \text{for } x \equiv 4m^2/s > 1, \end{array}\right. , \\ g(0, s) &= -\frac{8}{9}\ln\frac{m_b}{\mu} - \frac{4}{9}\ln\frac{s}{m_b^2} + \frac{8}{27} + \frac{4}{9}i\pi. &(11) \end{aligned}$$

Here and in the following, $s = q^2$ with $q = p_+ + p_-$, where $p_\pm$ are the four-momenta of the leptons. The appearance of an imaginary part in $Y_{pert}(s)$ at $s > 4m^2$ corresponds to on-shell quarks. Below (section 4.2) we comment on the applicability of this equation in this region of s. Also the coefficient C_7 gets redefined as $C_7^{\text{eff}} = C_7 + C_5/3 - C_6$, since in the particular calculation scheme used to determine the coefficients C_i in table 2, the quark-level matrix element of the operators $\mathcal{O}_5$ and $\mathcal{O}_6$ also have a tensor part ([5] and references therein). Note that $\mathcal{O}_{10}$ does not mix with other operators due to parity conservation. This also reflects in that C_{10} does not renormalize, i.e. $\gamma_{i,10} = 0$ (see section 3.2.1).

Finally we get the following formal expression for the quark level matrix element:

$$\begin{aligned} \mathcal{M}(b \to s\ell^+\ell^-) &= \frac{G_F\alpha}{\sqrt{2}\pi} V_{ts}^* V_{tb} \Bigg[C_9^{\text{eff}}[\bar{s}\gamma_\mu \frac{1}{2}(1-\gamma^5)b][\bar{\ell}\gamma^\mu\ell] + C_{10}[\bar{s}\gamma_\mu\frac{1}{2}(1-\gamma^5)b][\bar{\ell}\gamma^\mu\gamma^5\ell] \\ &\qquad -2\frac{m_b}{m_B} C_7^{\text{eff}} \left(\bar{s} i\sigma_{\mu\nu}\frac{q^\nu}{s}\frac{1}{2}(1+\gamma^5)b\right)[\bar{\ell}\gamma^\mu\ell]\Bigg]. &(12) \end{aligned}$$

The lepton part has been factorized out, and we explicitly see the vector structure of $\mathcal{O}_{9V}$, the axial structure of $\mathcal{O}_{10A}$ and the tensor structure of $\mathcal{O}_{7\gamma}$.

4.2 Long distance effects and resonances

The expression eq.(9) for the quark loop effect (see fig.7c) yields reliable estimates for highly virtual quarks in the loop, that is for $q^2 \ll 4m^2$. In this region we can rely on pertubative QCD calculations, as we did in the previous section. However, the pertubative expression is not applicable in the vicinity of resonances, i.e. when $q^2 \sim 4m^2$. In this region of q^2 interactions between quarks become strong, which manifests itself in the existence of resonances. This complicates things, since reliable calculations in the region of resonances can not be made perturbatively.

Loops of all but the c-quark are negligible, which can be seen from the expression for the loop function g in eq.11. Here only the $c\bar{c}$-loop gets a contribution from the large coefficients C_1 and C_2, whereas the others only include C_3-C_6 even with some cancellations (see table 2). Also, the $b\bar{b}$-states are much to heavy to have any influence. Since the only states of importance are the $c\bar{c}$-resonances, we should include J/ψ, ψ' and other charmonium states, which we have done by relying on phenomenology. Following [9], we have added a Breit-Wigner type contribution for all known $c\bar{c}$-resonances to the pertubative loop as follows:

$$Y_{full}(s) = Y_{pert}(s) + \frac{3\pi}{\alpha^2} C^{(0)} \sum_{\psi_i = J/\psi, \psi', \ldots, \psi(4415)} \kappa_i \frac{\Gamma(\psi_i \to \ell^+\ell^-) m_{\psi_i}}{m_{\psi_i}^2 - s m_B - i m_{\psi_i} \Gamma_{\psi_i}}, \tag{13}$$

where $C^{(0)} \equiv 3C_1 + C_2 + 3C_3 + C_4 + 3C_5 + C_6$, and the ψ-masses are listed in section 7.1.3. Note that α is taken at the scale m_ψ, differing from [1]. The factors of 3 in front of C_1, C_3 and C_5 in $C^{(0)}$ are due to the colour structure of their corresponding operators (see table 1). When the $q\bar{q}$-loop can have any colour (i.e. when it is disconnected from and thus independent of the bs-colour flow) we get three equal contributions.

The form of eq.(13) assumes a factorization of $B \to K^{(*)}\psi_i$ into a $B \to K^{(*)}$-transition and a ψ_i-decay constant. The factors κ_i (fudge factors) in eq.(13) adjust this approximation to the experimentally measured amplitudes $B \to J/\psi K^{(*)}$ and $B \to \psi' K^{(*)}$, that is they take into account the contributions from gluon exchange between the two parts (see figure in table 3), which are neglected in the factorization. The values of the fudge factors are listed in table 3 below:

κ	J/ψ	ψ'
K	2.70	3.51
K^*	1.65	2.36

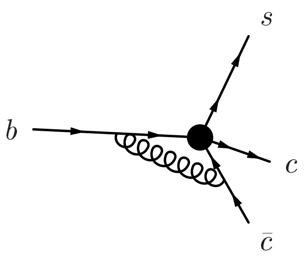

Table 3: Fudge factors in $B \to J/\psi K^{(*)}$ and $B \to \psi' K^{(*)}$. The values reflect the relative contribution to these decays from the non-factorizable diagrams, of which we have shown a lowest order example.

Since experimental data is missing for the remaining $c\bar{c}$-resonances, we have for these used an average of the ones for J/ψ and ψ' and averaged over charged and neutral data if available, following the same procedure as in [1].

At this point a word of warning seems proper. In addition to the pertubative calculation of quark loop effects, we have added a sum of Breit-Wigner resonance contributions. This is somewhat double counting, since the quark-antiquark and the hadronic states are dual. A more systematic way to include long distance effects is to use the hadronic dispersion relation for $Y(s)$, which is then normalized to the pertubative calculation in the low region of q^2, since the calculations there gives reliable results[7].

4.3 Hadronic matrix element and form factors

The quark level matrix element eq.(12) can easily be cast into a hadronic matrix element for the exclusive decay, by replacing quark spinors in eq.(12) by corresponding quark operators sandwiched between initial and final hadronic states:

$$\begin{aligned}\mathcal{M}(B \to K^{(*)}\ell^+\ell^-) &= \frac{G_F\alpha}{\sqrt{2}\pi}V_{ts}^*V_{tb}\Big[C_9^{\text{eff}} < K^{(*)}(p_K)|\bar{s}\gamma_\mu(1-\gamma^5)b|B(p_B) > [\bar{\ell}\gamma^\mu\ell] \\ &+ C_{10} < K^{(*)}(p_K)|\bar{s}\gamma_\mu(1-\gamma^5)b|B(p_B) > [\bar{\ell}\gamma^\mu\gamma^5\ell] \\ &- 2\frac{m_b}{m_B} < K^{(*)}(p_K)|\bar{s}\sigma_{\mu\nu}q^\nu(1+\gamma^5)b|B(p_B) > [\bar{\ell}\gamma^\mu\ell]\Big]. \end{aligned} \tag{14}$$

The calculation of the matrix elements should include all quark-gluon interactions with momenta lower than the factorization scale μ.

The hadronic matrix elements are parameterized by so called form factors, that is Lorentz-invariant functions of momentum transfer, s. For the $B \to K\ell^+\ell^-$ decay, this is done as follows [1], [12]:

$$\begin{aligned}< K(p_K)|\bar{s}\gamma_\mu(1-\gamma^5)b|B(p_B) > &= < K(p_K)|\bar{s}\gamma_\mu b|B(p_B) > \\ &= f_+(s)(p_B+p_K)_\mu + f_-(s)(p_B-p_K)_\mu, \end{aligned} \tag{15}$$

$$\begin{aligned}< K(p_K)|\bar{s}\sigma_{\mu\nu}q^\nu(1+\gamma^5)b|B(p_B) > &= < K(p_K)|\bar{s}\sigma_{\mu\nu}q^\nu b|B(p_B) > \\ &= i\left[s(p_B+p_K)_\mu - (m_B^2-m_K^2)q_\mu\right]\frac{f_T(s)}{m_B+m_K}. \end{aligned} \tag{16}$$

The axial part does not contribute in the $B \to K\ell^+\ell^-$ decay, which can be seen by analyzing the parity in the decay. Both $[\bar{s}\gamma_\mu\gamma^5 b]$ and $[\bar{s}\sigma_{\mu\nu}q^\nu\gamma^5 b]$ are axial vectors with positive parity. The B and the K are pseudoscalar mesons, and to construct a vector from them, one needs orbital momentum $L = 1$. But then the parity of the state would be negative, since the orbital momentum contributes with a factor $(-1)^L$, and so only the vector part contributes.

For the $B \to K^*\ell^+\ell^-$-decay there are more form factors, since the K^* also has a polarization vector ϵ_μ, and here the axial part contributes. The form factors can be divided into three categories - vector, axial and tensor form factors. The four axial and the one vector form factors A_0, A_1, A_2, A_3 and V are defined by:

$$\begin{aligned}< K^*(p_K)|\bar{s}\gamma_\mu(1-\gamma^5)b|B(p_B) > &= -i\epsilon_\mu^*(m_B+m_K^*)A_1(s) + i(p_B+p_K)_\mu(\epsilon^*\cdot p_B)\frac{A_2(s)}{m_B+m_K^*} \\ &+iq_\mu(\epsilon^*\cdot p_B)\frac{2m_{K^*}}{s}(A_3(s)-A_0(s)) \\ &+\epsilon_{\mu\nu\rho\sigma}\epsilon^{*\nu}p_B^\rho p_K^\sigma\frac{2V(s)}{m_B+m_K^*}. \end{aligned} \tag{17}$$

Some relations between the different form factors exist, and so only three of the axial form factors

[7]Some work is currently being done [10] to include non-factorizable contributions to $Y(s)$ and to avoid phenomenological fudge factors. In factorizable approximations, the dispersion approach has been applied in [11].

are independent:

$$\begin{aligned} A_3(s) &= \frac{m_B + m_{K^*}}{2m_{K^*}} A_1(s) - \frac{m_B - m_{K^*}}{2m_{K^*}} A_2(s), && (18) \\ A_0(0) &= A_3(0), && (19) \\ < K^*|\partial_\mu A^\mu|B > &= 2m_{K^*}(\epsilon^* \cdot p_B) A_0(s). && (20) \end{aligned}$$

The tensor form factors T_1, T_2 and T_3 are defined as follows:

$$\begin{aligned} < K^*(p_{K^*})|\bar{s}\sigma_{\mu\nu}q^\nu(1+\gamma^5)b|B(p_B) > &= i\epsilon_{\mu\nu\rho\sigma}\epsilon^{*\nu}p_B^\rho p_K^\sigma 2T_1(s) \\ &+ T_2(s)\left[\epsilon^*_\mu(m_B^2 - m_{K^*}^2) - (\epsilon^* \cdot p_B)(p_B + p_K)_\mu\right] \\ &+ T_3(s)(\epsilon^* \cdot p_B)\left[q_\mu - \frac{s}{m_B^2 - m_{K^*}^2}(p_B + p_K)_\mu\right], \quad (21) \end{aligned}$$

with the relation

$$T_1(0) = T_2(0). \quad (22)$$

The form factors can to some extent be calculated by approximate methods in QCD, but these calculations lie beyond the scope of this work, and we shall merely use the results, refering to the literature for details.

One procedure is to use the method of Light Cone QCD Sum Rules (LCSR), which was applied e.g. to the $B \to K^*\ell^+\ell^-$ form factor in [13]. For a general review of B-decay form factors, we refer to [12]. The results for all $B \to K^{(*)}\ell^+\ell^-$ form factors entering the defining equations (15)-(17) and (21) can be very well approximated with an exponential fit, which is what we have used in the numerical calculations (see section 7.1.2).

The results of this procedure compares well with lattice QCD calculations [14], and they also agree with the experimental restrictions that exist on C_7 from the CLEO measurement of $B \to K^*\gamma$ [2] (which only have contributions from C_7). Typical uncertainties on LCSR form factors range from 15% to 30%.

5 The $\mathbf{B} \to \mathbf{K}\ell^+\ell^-$ decay distribution

Given this matrix element, we can now compute the decay distributions of $B \to K\ell^+\ell^-$ and $B \to K^*\ell^+\ell^-$ by first squaring the element and then performing an integral over phase space. In the following we will do this in detail for the case of $B \to K\ell^+\ell^-$, which contains all the essential features. The case $B \to K^*\ell^+\ell^-$ will be treated in following section.

5.1 The squared matrix element $\mathcal{M}(\mathbf{B} \to \mathbf{K}\ell^+\ell^-)$

The matrix element eq.(14) can be rewritten to a more transparent form by splitting it into vector and axial current parts:

$$\mathcal{M} = \frac{G_F\,\alpha\, m_B}{2\sqrt{2}\pi}\; V_{ts}^* V_{tb}\;\left[\mathcal{T}_\mu{}^1(\bar{\ell}_-\gamma^\mu\ell_+) + \mathcal{T}_\mu{}^2(\bar{\ell}_-\gamma^\mu\gamma^5\ell_+)\right]. \quad (23)$$

$\mathcal{T}_\mu^1$ and $\mathcal{T}_\mu^2$ both depend on p_μ and q_μ separately, and one can then separate into two terms:

$$\mathcal{T}_\mu^1 = \frac{1}{m_B}(A'(\hat{s})p_\mu + B'(\hat{s})q_\mu), \quad \mathcal{T}_\mu^2 = \frac{1}{m_B}(C'(\hat{s})p_\mu + D'(\hat{s})q_\mu), \quad (24)$$

where $p \equiv p_B + p_K$, $q \equiv p_- + p_+ = p_B - p_K$. The coefficients A', B', C' and D' are expressed in terms of the form factors f_+, f_- and f_T and the Wilson coefficients $C_7^{\text{eff}}, C_9^{\text{eff}}$ and C_{10} (see section 4) in the following way:

$$A'(s) = C_9^{\text{eff}}(s) f_+(s) + \frac{2m_b}{m_B + m_K} C_7^{\text{eff}} f_T(s), \tag{25}$$

$$B'(s) = C_9^{\text{eff}}(s) f_-(s) + \frac{2m_b}{s}(m_B - m_K) C_7^{\text{eff}} f_T(s), \tag{26}$$

$$C'(s) = C_{10} f_+(s), \tag{27}$$

$$D'(s) = C_{10} f_-(s). \tag{28}$$

From this we can compute the square of the matrix element, which we need in order to calculate the partial width of this decay. We get:

$$\begin{aligned} |\mathcal{M}|^2 = \frac{G_F^2 \alpha^2 m_B^2}{8\pi^2} |V_{ts}^* V_{tb}|^2 \big(& \mathcal{T}_\mu^1 \mathcal{T}_\nu^{1*} (\bar{\ell}_- \gamma^\mu \ell_+)(\bar{\ell}_- \gamma^\nu \ell_+)^* + \mathcal{T}_\mu^1 \mathcal{T}_\nu^{2*} (\bar{\ell}_- \gamma^\mu \ell_+)(\bar{\ell}_- \gamma^\nu \gamma^5 \ell_+)^* \\ & + \mathcal{T}_\mu^2 \mathcal{T}_\nu^{1*} (\bar{\ell}_- \gamma^\mu \gamma^5 \ell_+)(\bar{\ell}_- \gamma^\nu \ell_+)^* + \mathcal{T}_\mu^2 \mathcal{T}_\nu^{2*} (\bar{\ell}_- \gamma^\mu \gamma^5 \ell_+)(\bar{\ell}_- \gamma^\nu \gamma^5 \ell_+)^* \big). \end{aligned} \tag{29}$$

Simple algebra gives:

$$(\bar{\ell}_- \gamma^\mu \ell_+)^* = (\bar{\ell}_+ \gamma^\mu \ell_-), \quad (\bar{\ell}_- \gamma^\mu \gamma^5 \ell_+)^* = (\bar{\ell}_+ \gamma^\mu \gamma^5 \ell_-). \tag{30}$$

Since the polarization of the leptons in the final state is not detected, we should sum over their spins:

$$\begin{aligned} \overline{|\mathcal{M}|}^2 = & \frac{G_F^2 \alpha^2 m_B^2}{8\pi^2} |V_{ts}^* V_{tb}|^2 \\ & \sum_{spin} \Big(\mathcal{T}_\mu^1 \mathcal{T}_\nu^{1*} (\bar{\ell}_-^{(s)} \gamma^\mu \ell_+^{(s')} \bar{\ell}_+^{(s)} \gamma^\nu \ell_-^{(s')}) + \mathcal{T}_\mu^1 \mathcal{T}_\nu^{2*} (\bar{\ell}_-^{(s)} \gamma^\mu \ell_+^{(s')} \bar{\ell}_+^{(s)} \gamma^\nu \gamma^5 \ell_-^{(s')}) \\ & + \mathcal{T}_\mu^2 \mathcal{T}_\nu^{1*} (\bar{\ell}_-^{(s)} \gamma^\mu \gamma^5 \ell_+^{(s')} \bar{\ell}_+^{(s)} \gamma^\nu \ell_-^{(s')}) + \mathcal{T}_\mu^2 \mathcal{T}_\nu^{2*} (\bar{\ell}_-^{(s)} \gamma^\mu \gamma^5 \ell_+^{(s')} \bar{\ell}_+^{(s)} \gamma^\nu \gamma^5 \ell_-^{(s)}) \Big). \end{aligned} \tag{31}$$

Using the identities (taking ℓ_- to be the lepton and ℓ_+ to be the antilepton):

$$\sum_{s=1,2} \ell_-^{(s)}(p_-) \bar{\ell}_-^{(s)}(p_-) = \not{p}_- + m_\ell, \qquad \sum_{s=1,2} \ell_+^{(s)}(p_+) \bar{\ell}_+^{(s)}(p_+) = \not{p}_+ - m_\ell, \tag{32}$$

we obtain

$$\begin{aligned} \overline{|\mathcal{M}|}^2 = & \frac{G_F^2 \alpha^2 m_B^2}{8\pi^2} |V_{ts}^* V_{tb}|^2 \\ & \big(\mathcal{T}_\mu^1 \mathcal{T}_\nu^{1*} Tr[(\not{p}_- + m_\ell)\gamma^\mu(\not{p}_+ - m_\ell)\gamma^\nu] + \mathcal{T}_\mu^1 \mathcal{T}_\nu^{2*} Tr[(\not{p}_- + m_\ell)\gamma^\mu(\not{p}_+ - m_\ell)\gamma^\nu\gamma^5] + \\ & \mathcal{T}_\mu^2 \mathcal{T}_\nu^{1*} Tr[(\not{p}_- + m_\ell)\gamma^\mu\gamma^5(\not{p}_+ - m_\ell)\gamma^\nu] + \mathcal{T}_\mu^2 \mathcal{T}_\nu^{2*} Tr[(\not{p}_- + m_\ell)\gamma^\mu\gamma^5(\not{p}_+ - m_\ell)\gamma^\nu\gamma^5] \big). \end{aligned} \tag{33}$$

To evaluate the traces, we use the following well known rules for traces of γ-matrices:

$$Tr[\gamma^\rho \gamma^\mu \gamma^\sigma \gamma^\nu] = 4(g^{\rho\mu} g^{\sigma\nu} + g^{\rho\nu} g^{\sigma\mu} - g^{\rho\sigma} g^{\mu\nu}), \tag{34}$$

$$Tr[\gamma^\rho \gamma^\mu \gamma^\sigma \gamma^\nu \gamma^5] = -4i\epsilon^{\rho\mu\sigma\nu}, \tag{35}$$

$$Tr[\gamma^\rho \gamma^\mu \gamma^5 \gamma^\sigma \gamma^\nu \gamma^5] = Tr[\gamma^\rho \gamma^\mu \gamma^\sigma \gamma^\nu] \tag{36}$$

Neglecting the lepton mass, which for $\ell \neq \tau$ is tiny relative to the other masses involved in the problem, we get using eqs. (34)-(36):

$$\begin{aligned}
\overline{|\mathcal{M}|}^2 &= \frac{G_F^2\alpha^2 m_B^2}{8\pi^2}|V_{ts}^*V_{tb}|^2 \left(\mathcal{T}_\mu^1\mathcal{T}_\nu^{1*}\ Tr[\gamma^\rho\gamma^\mu\gamma^\sigma\gamma^\nu]p_\rho p_\sigma + \mathcal{T}_\mu^1\mathcal{T}_\nu^{2*}\ Tr[\gamma^\rho\gamma^\mu\gamma^\sigma\gamma^\nu\gamma^5]p_\rho p_\sigma\right.\\
&\quad \left. + \mathcal{T}_\mu^2\mathcal{T}_\nu^{1*}\ Tr[\gamma^\rho\gamma^\mu\gamma^5\gamma^\sigma\gamma^\nu]p_\rho^- p_\sigma^+ + \mathcal{T}_\mu^2\mathcal{T}_\nu^{2*}\ Tr[\gamma^\rho\gamma^\mu\gamma^5\gamma^\sigma\gamma^\nu\gamma^5]p_\rho^- p_\sigma^+\right).\\
&= \frac{G_F^2\alpha^2 m_B^2}{2\pi^2}|V_{ts}^*V_{tb}|^2 \left(\mathcal{T}_\mu^1\mathcal{T}_\nu^{1*}\ (g^{\rho\mu}g^{\sigma\nu} + g^{\rho\nu}g^{\sigma\mu} - g^{\rho\sigma}g^{\mu\nu})p_\rho^- p_\sigma^+ - i\mathcal{T}_\mu^1\mathcal{T}_\nu^{2*}\ \epsilon^{\rho\mu\sigma\nu}p_\rho^- p_\sigma^+\right.\\
&\quad \left. - i\mathcal{T}_\mu^2\mathcal{T}_\nu^{1*}\ \epsilon^{\rho\mu\sigma\nu}p_\rho^- p_\sigma^+ + \mathcal{T}_\mu^2\mathcal{T}_\nu^{2*}\ (g^{\rho\mu}g^{\sigma\nu} + g^{\rho\nu}g^{\sigma\mu} - g^{\rho\sigma}g^{\mu\nu})p_\rho^- p_\sigma^+\right).\\
&= \frac{G_F^2\alpha^2 m_B^2}{2\pi^2}|V_{ts}^*V_{tb}|^2 \left[\mathcal{T}_\mu^1\mathcal{T}_\nu^{1*} + \mathcal{T}_\mu^2\mathcal{T}_\nu^{2*}\right](p_-^\mu p_+^\nu + p_-^\nu p_+^\mu - (p_-\cdot p_+)g^{\mu\nu}).
\end{aligned} \tag{37}$$

The $\mathcal{T}_\mu^1\mathcal{T}_\nu^{2*} + \mathcal{T}_\mu^2\mathcal{T}_\nu^{1*}$ term vanishes, since $\epsilon^{\rho\mu\sigma\nu}$ is antisymmetric in all indices and there are only three independent momenta, thus a combination of four momenta will be symmetric in two indices. Physically, this is because a vector current and an axial current can not mix.

Inserting the definitions eq.(24) of $\mathcal{T}_\mu^1$ and $\mathcal{T}_\mu^2$ into eq.(37), the terms containing B' and D' vanish. The equation of motion of lepton fields makes the B' term vanish, and the D' term drops out, since q dotted into the lepton current gives terms proportional to the lepton mass squared, which we have decided to neglect. This leaves us with:

$$\overline{|\mathcal{M}|}^2 = \frac{G_F^2\alpha^2}{2\pi^2}|V_{ts}^*V_{tb}|^2(|A'|^2+|C'|^2)p_\mu p_\nu(p_-^\mu p_+^\nu + p_-^\nu p_+^\mu - (p_-\cdot p_+)g^{\mu\nu}). \tag{38}$$

It turns out to be advantageous to rewrite p_+ and p_- in terms of q and r defined by:

$$q \equiv p_- + p_+,\quad r \equiv p_- - p_+ \quad \Rightarrow \quad p_- = (q+r)/2,\quad p_+ = (q-r)/2, \tag{39}$$

from which we have (still neglecting the lepton mass):

$$q\cdot r = 0,\quad p_-\cdot p_+ = s/2. \tag{40}$$

Inserting this into eq.(38) gives:

$$\begin{aligned}
\overline{|\mathcal{M}|}^2 &= \frac{G_F^2\alpha^2}{8\pi^2}|V_{ts}^*V_{tb}|^2(|A'|^2+|C'|^2)\ p_\mu p_\nu(2q^\mu q^\nu - 2r^\mu r^\nu - 4(p_-\cdot p_+)g^{\mu\nu}).\\
&= \frac{G_F^2\alpha^2}{4\pi^2}|V_{ts}^*V_{tb}|^2(|A'|^2+|C'|^2)\ ((p\cdot q)^2 - (p\cdot r)^2 - sp^2).
\end{aligned} \tag{41}$$

The first two dot products are:

$$p\cdot q = (p_B + p_K)\cdot(p_B - p_K) = m_B^2 - m_K^2, \tag{42}$$

$$p\cdot r = (2p_B - q)\cdot r = 2p_B\cdot r = -u, \tag{43}$$

where in the last expression we have defined a Mandelstam-type variable u as follows[8]:

$$u \equiv (p_B - p_-)^2 - (p_B - p_+)^2 = -2p_B\cdot p_- + 2p_B\cdot p_+ = -2p_B\cdot r. \tag{44}$$

The last dot product in eq.(41) is

$$s = q^2 = (p_B - p_K)^2 = m_B^2 + m_K^2 - 2p_B\cdot p_K, \quad \Rightarrow \tag{45}$$

$$p^2 = (p_B + p_K)^2 = m_B^2 + m_K^2 + 2p_B\cdot p_K = 2m_B^2 + 2m_K^2 - s. \tag{46}$$

[8]The usual definition in processes of the type $A + B \to C + D$ is $u \equiv (p_A - p_D)^2$.

Inserting in the expression for $\overline{|\mathcal{M}|}^2$ eq.(41) gives:

$$\begin{aligned}\overline{|\mathcal{M}|}^2 &= \frac{G_F^2\alpha^2}{4\pi^2}|V_{ts}^*V_{tb}|^2(|A'|^2+|C'|^2)\left((m_B^2-m_K^2)^2-u^2-s(2m_B^2+2m_K^2-s)\right)\\ &= \frac{G_F^2\alpha^2}{4\pi^2}|V_{ts}^*V_{tb}|^2(|A'|^2+|C'|^2)\left(\lambda(m_B^2,m_K^2,s)-u^2\right),\end{aligned} \tag{47}$$

where we have employed the following common definition:

$$\lambda(m_B^2,m_K^2,s) \equiv m_B^4+m_K^4+s^2-2m_B^2m_K^2-2m_B^2s-2m_K^2s. \tag{48}$$

5.2 The decay distribution, $d\Gamma^K(\mathbf{B} \to \mathbf{K}\ell^+\ell^-)$

The decay distribution for a three-body decay is:

$$d\Gamma^K \equiv \frac{\overline{|\mathcal{M}|}^2}{2m_B}\frac{d^3p_K}{(2\pi)^3 2E_K}\frac{d^3p_1}{(2\pi)^3 2E_1}\frac{d^3p_2}{(2\pi)^3 2E_2}(2\pi)^4\delta^{(4)}(p_B-p_K-p_1-p_2). \tag{49}$$

This can be rewritten by dividing the three body phase space into two two-body phase spaces, by inserting the identity:

$$\int d^4q\ \delta^{(4)}(q-p_1-p_2)=1, \tag{50}$$

which gives us:

$$\begin{aligned}d\Gamma^K &= \frac{1}{2\pi}\int 2q_0dq_0\frac{\overline{|\mathcal{M}|}^2}{2m_B}\left[\frac{d^3p_K}{(2\pi)^3 2E_K}\frac{d^3q}{(2\pi)^3 2q_0}(2\pi)^4\delta^{(4)}(p_B-p_K-q)\right]\\ &\left[\frac{d^3p_1}{(2\pi)^3 2E_1}\frac{d^3p_2}{(2\pi)^3 2E_2}(2\pi)^4\delta^{(4)}(q-p_1-p_2)\right].\end{aligned} \tag{51}$$

Each two-body phase space can be simplified separately:

$$\frac{d^3p_K}{(2\pi)^3 2E_K}\frac{d^3q}{(2\pi)^3 2q_0}(2\pi)^4\delta^{(4)}(p_B-p_K-q) = \sqrt{\lambda(m_B^2,m_K^2,s)}\frac{1}{8\pi\ m_B^2}, \tag{52}$$

$$\frac{d^3p_1}{(2\pi)^3 2E_1}\frac{d^3p_2}{(2\pi)^3 2E_2}(2\pi)^4\delta^{(4)}(q-p_1-p_2) = \frac{1}{8(2\pi)^2}d\cos\theta\ d\phi\ dE_1\delta(\frac{m_B}{2}-E_1) = \frac{1}{16\pi}d\cos\theta. \tag{53}$$

The second two-body phase space expression eq.(53) can be further simplified by choosing the angle θ to be the angle between the B-meson and the negatively charged lepton *in the CM frame of the leptons* (define $\vec{p}_\ell \equiv \vec{p}_{\ell^-} = -\vec{p}_{\ell^+}$), since we can then express the variable u in terms of θ_{B,ℓ^-}:

$$u = (p_B-p_-)^2-(p_B-p_+)^2 = 2p_B\cdot(p_+-p_-) = 2|\vec{p}_B||\vec{p}_\ell|\cos\theta_{B,\ell^-}. \tag{54}$$

From energy and momentum conservation we get:

$$\sqrt{|\vec{p}_B|^2+m_B^2}-\sqrt{|\vec{p}_K|^2+m_K^2}=\sqrt{s} \ \Rightarrow\ |\vec{p}_B| = \frac{\sqrt{\lambda(m_B^2,m_K^2,s)}}{2\sqrt{s}}, \tag{55}$$

$$\sqrt{|\vec{p}_\ell|^2+m_\ell^2}+\sqrt{|\vec{p}_\ell|^2+m_\ell^2}=\sqrt{s} \ \Rightarrow\ |\vec{p}_\ell| = \frac{\sqrt{s}}{2}\sqrt{1-\frac{4m_\ell^2}{s}}, \tag{56}$$

which inserted in eq.(54) gives:

$$u = \sqrt{\lambda(m_B^2, m_K^2, s)\left(1 - \frac{4m_\ell^2}{s}\right)} \cos\theta_{B,\ell^-} \quad \Rightarrow \quad du \doteq \sqrt{\lambda(m_B^2, m_K^2, s)} d\cos\theta_{B,\ell^-}, \tag{57}$$

where, in the last expression, we have neglected the lepton mass term. This leads us to:

$$\frac{1}{16\pi} d\cos\theta_{B,\ell^-} = \frac{1}{16\pi} \frac{1}{\sqrt{\lambda(m_B^2, m_K^2, s)}} du. \tag{58}$$

Inserting the two two-body phase space expressions in eq.(51) gives:

$$\begin{aligned} d\Gamma^K &= \frac{1}{2\pi} \int ds \frac{\overline{|\mathcal{M}|}^2}{2m_B} \frac{\sqrt{\lambda(m_B^2, m_K^2, s)}}{8\pi\, m_B^2} \frac{1}{16\pi} \frac{1}{\sqrt{\lambda(m_B^2, m_K^2, s)}} du, \\ &= \int \frac{\overline{|\mathcal{M}|}^2}{2^9 \pi^3 m_B^3} ds du. \end{aligned} \tag{59}$$

Now we can insert the square of the matrix element eq.(47) which in turn gives the following differential decay distribution:

$$\frac{d\Gamma^K}{ds du} = \frac{G_F^2 \alpha^2}{2^{11} \pi^5 m_B^3} |V_{ts}^* V_{tb}|^2 (|A'|^2 + |C'|^2) \left[\lambda(m_B^2, m_K^2, s) - u^2\right]. \tag{60}$$

This result agrees with [1][9].

5.3 The $\mathbf{B} \to \mathbf{K}^*\ell^+\ell^-$ decay

The computation of the square of the matrix element for $B \to K^*\ell^+\ell^-$ is in principle no more complicated than the one for $B \to K\ell^+\ell^-$, which we just did in detail (see 5.1). However, the calculation is much more tedious, since after casting the matrix elements in the convenient form of eq.(23) one obtains more complicated expressions for $\mathcal{T}_\mu^1$ and $\mathcal{T}_\mu^2$. They are obtained by substitution of eqs. (15)-(17) and (21) into eq.(14):

$$\mathcal{T}_\mu^1 = A(\hat{s}) \epsilon_{\mu\rho\alpha\beta} \epsilon^{*\rho} \frac{p_B^\alpha p_{K^*}^\beta}{m_B^2} + iB(\hat{s}) \epsilon_\mu^* + iC(\hat{s}) \frac{(\epsilon^* \cdot p_B) p_\mu}{m_B^2} + iD(\hat{s}) \frac{(\epsilon^* \cdot p_B) q_\mu}{m_B^2}, \tag{61}$$

$$\mathcal{T}_\mu^2 = E(\hat{s}) \epsilon_{\mu\rho\alpha\beta} \epsilon^{*\rho} \frac{p_B^\alpha p_{K^*}^\beta}{m_B^2} + iF(\hat{s}) \epsilon_\mu^* + iG(\hat{s}) \frac{(\epsilon^* \cdot p_B) p_\mu}{m_B^2} + iH(\hat{s}) \frac{(\epsilon^* \cdot p_B) q_\mu}{m_B^2}. \tag{62}$$

[9]Note that the authors in [1] use rescaled variables, e.g. $\hat{s} \equiv s/m_b^2$.

The coefficients A, B, C, D, E, F, G and H are:

$$A(s) = \frac{2m_B}{m_B + m_{K^*}} C_9^{\text{eff}}(s) V + \frac{4m_b m_B}{s} C_7^{\text{eff}} T_1, \tag{63}$$

$$B(s) = \frac{m_B + m_{K^*}}{m_B} \left[C_9^{\text{eff}}(s) A_1 + \frac{2m_b(m_B - m_{K^*})}{s} C_7^{\text{eff}} T_2 \right], \tag{64}$$

$$C(s) = \frac{m_B^2}{m_B^2 - m_{K^*}^2} \left[\frac{m_B - m_{K^*}}{m_B} C_9^{\text{eff}}(s) A_2 + \frac{2m_b}{m_B} C_7^{\text{eff}} \left(T_3 + \frac{m_B^2 - m_{K^*}^2}{s} T_2 \right) \right], \tag{65}$$

$$D(s) = \frac{m_B^2}{s} \left[C_9^{\text{eff}}(s) \left(\frac{m_B + m_{K^*}}{m_B} A_1 - \frac{m_B - m_{K^*}}{m_B} A_2 - \frac{2m_{K^*}}{m_B} A_0 \right) - \frac{2m_b}{m_B} C_7^{\text{eff}} T_3 \right], \tag{66}$$

$$E(s) = \frac{2m_B}{m_B + m_{K^*}} C_{10}(s) V, \tag{67}$$

$$F(s) = \frac{m_B + m_{K^*}}{m_B} C_{10}(s) A_1, \tag{68}$$

$$G(s) = \frac{m_B}{m_B + m_{K^*}} C_{10}(s) A_2, \tag{69}$$

$$H(s) = \frac{m_B^2}{s} C_{10}(s) \left[\frac{m_B + m_{K^*}}{m_B} A_1 - \frac{m_B - m_{K^*}}{m_B} A_2 - \frac{2m_{K^*}}{m_B} A_0 \right], \tag{70}$$

where the s-dependence of the form factors is omitted for brevity.

Fortunately, there exist programs to handle such calculations. A particularly simple one is `FORM` [15], which evaluates traces, contracts indices and simplifies expressions. We have computed $|\mathcal{M}(B \to K^* \ell^+ \ell^-)|^2$ with `FORM`, since the time saved in doing it this way, gives no lack of generality of calculating these matrix elements. The source code for the program to do the calculation in `FORM` can be found in appendix A. One has to define *symbols* (constants, Mandelstam variables), *vectors* (momenta, polarizations) and *indices*, and then write the expression to evaluate.

From the matrix element one can calculate the decay distribution in exactly the same way as before, since the kinematics are the same, only m_K should be changed to m_{K^*}. The result of this process for the $B \to K^* \ell^+ \ell^-$ decay is:

$$\begin{aligned} \frac{d\Gamma^{K^*}}{ds du} = {} & \frac{G_F^2 \alpha^2}{2^{11} \pi^5 m_B^3} |V_{ts}^* V_{tb}|^2 \left[\frac{(|A|^2 + |E|^2)}{4} \frac{s}{m_B^2} (\lambda + u^2) + \frac{m_B^2}{4m_{K^*}^2} (|B|^2 + |F|^2)(\lambda - u^2 + 8m_{K^*}^2 s) \right. \\ & - 2su(Re(AF^*) + Re(BE^*)) + \frac{\lambda}{4m_{K^*}^2 m_B^2} (|C|^2 + |G|^2)(\lambda - u^2) \\ & \left. - \frac{1}{2m_{K^*}^2} (Re(BC^*) + Re(FG^*))(m_B^2 - m_{K^*}^2 - s)(\lambda - u^2) \right]. \end{aligned} \tag{71}$$

This result coincides with [1] up to several terms proportional to the square of the lepton masses, which we neglect in this formula. However, using `FORM` it is straight forward to include these terms, and in the following calculation of spectra, we have used the full expressions.

5.4 Dilepton invariant mass spectra

Given the two differential decay distributions eq.(60) and eq.(71), we can integrate out the u-dependence and obtain expressions for the dilepton mass spectra. We denote the kinematical limits for u by $u_\pm(s)$, and they are obtained from eq.(57):

$$u_\pm(s) = \pm \sqrt{\lambda(m_B^2, m_K^2, s) \left(1 - \frac{4m_\ell^2}{s} \right)}, \tag{72}$$

i.e. the limit is symmetrical and depends on s, as it should. The actual integrations are straight forward, and the results for $B \to K\ell^+\ell^-$ and $B \to K^*\ell^+\ell^-$ are respectively:

$$\frac{d\Gamma^K}{ds} = \frac{G_F^2\alpha^2}{2^{10}\pi^5 m_B^3}|V_{ts}^* V_{tb}|^2(|A'|^2+|C'|^2)u_+(s)\left[\lambda(m_B^2, m_K^2, s) - \frac{(u_+(s))^2}{3}\right], \tag{73}$$

$$\begin{aligned}\frac{d\Gamma^{K^*}}{ds} &= \frac{G_F^2\alpha^2}{2^{10}\pi^5 m_B^3}|V_{ts}^* V_{tb}|^2 u_+(s)\left[\frac{(|A|^2+|E|^2)}{4}\frac{s}{m_B^2}(\lambda + \frac{(u_+(s))^2}{3})\right.\\ &+ \frac{m_B^2}{4m_{K^*}^2}(|B|^2+|F|^2)(\lambda - \frac{(u_+(s))^2}{3} + 8m_{K^*}^2 s) - su_+(s)(Re(AF^*) + Re(BE^*))\\ &+\frac{\lambda}{4m_{K^*}^2 m_B^2}(|C|^2+|G|^2)(\lambda - \frac{(u_+(s))^2}{3})\\ &\left. - \frac{1}{2m_{K^*}^2}(Re(BC^*) + Re(FG^*))(m_B^2 - m_{K^*}^2 - s)(\lambda - \frac{(u_+(s))^2}{3})\right].\end{aligned} \tag{74}$$

These results are again consistent with the results obtained in [1].

5.5 Forward-backward asymmetries

A quantity of interest is the differential *forward-backward asymmetry* (FBA) in the decay, which is defined [9] as:

$$\frac{d\mathcal{A}_{FB}}{ds} \equiv -\int_0^{u_\pm(s)}\frac{d^2\Gamma}{duds}du + \int_{-u_\pm(s)}^0 \frac{d^2\Gamma}{duds}du. \tag{75}$$

The FBA is the difference between ratio of B-mesons in the direction of the negative lepton ($\theta_{B,\ell^-} < \pi/2$) and ratio in the opposite hemisphere ($\theta_{B,\ell^-} > \pi/2$), in the CM-frame of the leptons. In the $B \to K\ell^+\ell^-$ decay the FBA vanishes, since the expression for the differential decay contains no odd powers of u eq.(60). However, this is not the case for the $B \to K^*\ell^+\ell^-$ decay eq.(71), where the FBA is:

$$\begin{aligned}\frac{d\mathcal{A}_{FB}}{ds} &= \frac{G_F^2\alpha^2}{2^{10}\pi^5 m_B^3}|V_{ts}^* V_{tb}|^2 s(u_+(s))^2[Re(AF^*) + Re(BE^*)]\\ &= \frac{G_F^2\alpha^2}{2^{10}\pi^5 m_B^3}|V_{ts}^* V_{tb}|^2 s(u_+(s))^2\\ &\quad C_{10}\left[Re(C_9^{\text{eff}} VA_1 + \frac{m_b}{s}C_7^{\text{eff}}(VT_2(1-\frac{m_{K^*}}{m_B}) + A_1T_1(1+\frac{m_{K^*}}{m_B}))\right],\end{aligned} \tag{76}$$

where we in the last equation have inserted the Wilson coefficients and the form factors discussed earlier. In order to cancel out systematic errors, experimentally one usually measures the normalized FBA defined as:

$$\frac{d\overline{\mathcal{A}_{FB}}}{ds} \equiv \frac{-\int_0^{u_\pm(s)}\frac{d^2\Gamma}{duds}du + \int_{-u_\pm(s)}^0\frac{d^2\Gamma}{duds}du}{+\int_0^{u_\pm(s)}\frac{d^2\Gamma}{duds}du + \int_{-u_\pm(s)}^0\frac{d^2\Gamma}{duds}du} = \frac{\frac{d\mathcal{A}_{FB}}{ds}}{\frac{d\Gamma}{ds}}. \tag{77}$$

The asymmetry is of course dependent on s, and turns out to have quite different behavior for various scenarios of physics. In addition asymmetries will be some of the best measured quantities experimentally, since many systematic errors cancel out in the subtraction and the ratio. Furthermore, the theoretical uncertainties on the form factors cancel to a large extent, as can be seen in fig.15. For these reasons, FBA in $B \to K^*\ell^+\ell^-$-decay is a good probe of new physics.

6 $\mathbf{B} \to \mathbf{K}^{(*)}\ell^+\ell^-$ in the Supergravity models

Among the candidate theories for physics beyond the SM, supersymmetry is generally considered the most promising. It is our purpose here to give a brief summary of the essential concepts involved and of the way in which they modify our results rather than to review the detailed workings of the theory. For such a review, the reader is referred to standard textbooks on the matter such as [16]. For the decays under consideration, we also refer to the study carried out in [1] and, for the supergravity model, to [17] whose calculations of Wilson coefficients have been used in this project. It is also mainly from these sources, along with the review presented in [4], that the following has been constructed.

6.1 Basics of supersymmetry

The basic idea of supersymmetry is that each particle should be accompanied by a superpartner of spin 1/2 less than the particle itself with the exception of the Higgs bosons (spin 0) whose superpartners are fermions of spin 1/2. The nomenclature is such that superpartners of fermions get the prefix s- (e.g. leptons $\to$ sleptons), while the gauge and Higgs bosons acquire the suffix -ino (e.g. gluon $\to$ gluino, higgs $\to$ higgsino). The notation is such that the symbol for a particle gets a tilde when symbolizing a superparticle, thus a squark is written symbolically as $\tilde{q}$.

In general, the supersymmetric models require a minimum of two Higgs doublets. In the following, only the two-doublet scenario is considered. These doublets (H_1, H_2) have neutral components with vacuum expectation values $(\langle h_1\rangle,\langle h_2\rangle)$ generating the masses in the physical particle spectrum. In addition, there are the massive higgs particles consisting of two charged bosons, $H^\pm$, two neutral scalars H_1^0, H_2^0, and one pseudoscalar, A, (See [4] for a review of the progress of current experimental searches). Note that the superpartners of these fields are fermionic with spin 1/2, the charged ones mixing with the charged gaugino field $\tilde{W}^\pm$ (also spin 1/2) to produce the chargino mass eigenstates $\tilde{\chi}_1^\pm$,$\tilde{\chi}_2^\pm$ and the neutral ones (apart from the $\tilde{A}^0$) mixing with the $\tilde{Z}$ and $\tilde{\gamma}$ (or, equivalently, $\tilde{B}$ and $\tilde{W}^0$) fields to produce the neutralino mass eignestates, $\tilde{\chi}_i$ $(i = 1-4)$.

6.2 Supergravity

The simplest supersymmetric scenario is that of supergravity where mass splitting at the soft scale[10] is introduced without regard for quark generation, the graviton being insensitive to the differences between quark generations and other quantum numbers. This is justified since too large FCNC rates would result, if arbitrary splittings and mixings were allowed [17]. Thus, all squark and slepton masses are assumed to be equal at the Planck scale[11], and likewise the Higgs mass terms are assumed equal. In the *minimal* case, there is the additional condition that the Higgs masses be equal to the squark/slepton masses at this scale. Equal masses at the Planck scale are also assigned to the gauge fields $\tilde{B}$, $\tilde{W}$, and $\tilde{G}$, where the mixing with the Higgsino fields to produce mass eigenstates was described above.

As mentioned, the neutral components of the Higgs doublets have vacuum expectation values $\langle h_1^0\rangle$ and $\langle h_2^0\rangle$, where the superscript zero indicates evaluation at the Planck scale. The ratio of these expectation values enters as the parameter $\tan\beta = \langle h_2^0\rangle / \langle h_1^0\rangle$ in the calculations performed in [17], where the effects on the Wilson coefficients C_7, C_9, and C_{10} of $\tan\beta = 30$ and $\tan\beta = 2$ models have been investigated for minimal as well as non-minimal supergravity. This range of $\tan\beta$ corresponds to the one usually considered in the literature, see e.g. [4].

[10] Scales much smaller than the Planck and GUT scales, $M_{Planck} \approx 10^{19}$GeV, $M_{GUT} \approx 2\times 10^{16}$GeV.
[11] The authors in [17] do not distinguish between the Planck and GUT scales.

6.3 FCNC processes in supergravity

Supersymmetric particles influence FCNC processes due to the loop structure of the FCNC diagrams. We do not observe supersymmetric particles in our detectors[12], and thus we have to "hide" the supersymmetric physics somewhere in the internal parts of the diagrams. In addition, a sort of corollary of supersymmetry is that the "supercurrent" has to be conserved in any given diagram due to a multiplicative quantum number called R-parity, $R = (-1)^{3*(B-L)+2S}$, where B,L and S is the baryon number, lepton number and spin, respectively, making all SM particles R-even and their superpartners R-odd, due to the difference in spins. If this quantity is conserved (there exist R-breaking models, yet we are not concerned with those here), then it follows that superparticles can only be produced from SM particles in pairs, i.e. we cannot simply exchange *one* line for a supersymmetric one without requiring that there be a loop of supersymmetric particles allowing the supercurrent to connect back to itself. It is here that the reason why FCNC processes are such eminent probes of supersymmetry becomes apparent: even the lowest order diagrams for these processes contain loops which can be replaced by supercurrents (illustrated in fig.8), and thus the potential effects of supersymmetry are much larger for these processes than for processes possible at the tree-level.

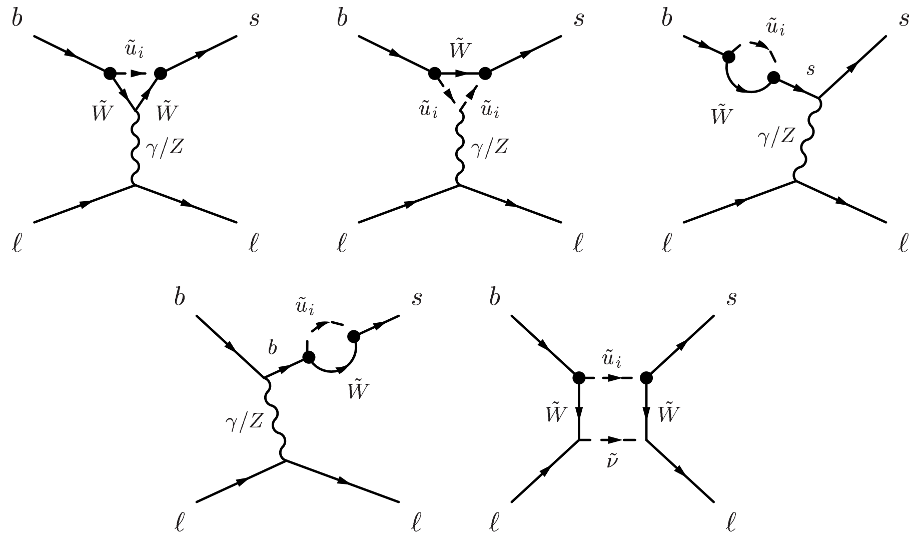

Figure 8: The penguin and box diagrams of fig.2 with their loops replaced by the corresponding supercurrents. Note that the $\tilde{u}_i$ and $\tilde{\nu}$ are scalars and that the $\tilde{W}$ represents the fermionic chargino fields.

As the differences between these diagrams and the ones presented for the SM in fig.2 are all to do with the internal parts, which we integrated into the C_i in section 3, their contributions can be included in the analysis by recalculating the C_i at the electroweak scale including the supersymmetric contributions, and once again using the Renormalization Group method to obtain the result at $\mu = m_b$. This is, in essence, what has been done in [17], and thus we have been able to include the effects of the models investigated in that article by allowing the C_i to vary within the limits of the parameter spaces obtained there. Note that, due to the general nature of supersymmetry, the SM result is usually contained in these parameter spaces, making it possible to rule out the SM in favour of supersymmetry, but not vice versa.

[12] At least current investigations at LEP put lower limits on the masses of superparticles which are about 100GeV.

7 Numerical calculations

All numerical calculations have been performed using `Mathematica` (see Appendix B for the full program). Note that the lepton mass has not been put to zero in these calculations[13], although we have been using $m_\ell = m_\mu$, and thus the results are valid for both $\ell = e, \mu$, but not for $\ell = \tau$. As stated in the previous section, the analytical results for non-zero lepton masses have been obtained using the `FORM` algebra engine.

7.1 Parameters

7.1.1 Constants and masses

The constants and masses entering the calculations have all been taken from the Particle Data Book [4]. They are as follows:

$$
\begin{array}{rcl}
m_K & = & 0.495\ \text{GeV} \\
m_{K^*} & = & 0.892\ \text{GeV} \\
m_B & = & 5.279\ \text{GeV} \\
m_\mu & = & 0.106\ \text{GeV} \\
m_\pi & = & 0.140\ \text{GeV} \\
 & & \\
m_b & = & 4.8\ \text{GeV} \\
m_c & = & 1.4\ \text{GeV}
\end{array}
\qquad
\begin{array}{rcl}
G_F & = & 1.166\ \text{GeV}^{-2} \\
\alpha(m_Z) & = & 129^{-1} \\
\alpha(m_\psi) & = & 137^{-1} \\
\alpha_s(m_b) & = & 0.2185
\end{array}
$$

Table 4: Masses and constants entering the calculations. It should be noted that the quark masses are affected by large theoretical uncertainties. To enable a comparison with [1], we have chosen values identical to those presented there. The renormalization scale used in all calculations is $\mu = m_b$.

7.1.2 Form factors

We have been using the form factors obtained from Light Cone Sum Rules (LCSR) in [1]. The parameterization used is:

$$F(\hat{s}) = F(0) \exp\left(c_1 \hat{s} + c_2 \hat{s}^2 + c_3 \hat{s}^3\right) \tag{78}$$

where $F(0)$, c_1, c_2, and c_3 for the relevant form factors are tabulated in table 5, 6, and 7 for the respective central, maximum and minimum allowed form factors within the theoretical uncertainty. As c_3 enters with s^3 in eq.(78), and as the decay $B \to K^* \ell^+ \ell^-$ has a lower kinematical upper limit due to the larger mass of the K^*, c_3 has been neglected in the form factors relevant to this decay. It should be noted that this parameterization is merely a fit, valid inside the region $2m_\ell^2 < s < (m_B - m_{K^{(*)}})^2$.

7.1.3 Resonances

For the ψ resonances entering C_9^{eff}, we have employed a phenomenological Breit-Wigner parameterization as described in section 4.2. The ψ masses and leptonic widths have been taken from the Particle Data Book [4] and are given in table 8.

[13] However, the effect of lepton masses is of course small for $\ell = e, \mu$.

	f_+	f_-	f_T	A_1	A_2	A_0	V	T_1	T_2	T_3
$F(0)$	0.319	0.319	0.355	0.337	0.282	0.471	0.457	0.379	0.379	0.260
c_1	1.465	0.633	1.478	0.602	1.172	1.505	1.482	1.519	0.517	1.129
c_2	0.372	-0.095	0.373	0.258	0.567	0.710	1.015	1.030	0.426	1.128
c_3	0.782	0.591	0.700	0	0	0	0	0	0	0

Table 5: Parameterization values for the central values of the form factors for $B \to K\ell^+\ell^-$ and $B \to K^*\ell^+\ell^-$. c_3 can be neglected for $B \to K^*\ell^+\ell^-$.

	f_+	f_-	f_T	A_1	A_2	A_0	V	T_1	T_2	T_3
$F(0)$	0.371	0.371	0.423	0.385	0.320	0.698	0.548	0.437	0.437	0.295
c_1	1.412	0.579	1.413	0.557	1.083	1.945	1.462	1.498	0.495	1.044
c_2	0.261	-0.240	0.247	0.068	0.393	0.314	0.953	0.976	0.402	1.378
c_3	0.822	0.774	0.742	0	0	0	0	0	0	0

Table 6: Maximum form factor parameterization values.

	f_+	f_-	f_T	A_1	A_2	A_0	V	T_1	T_2	T_3
$F(0)$	0.278	0.278	0.300	0.294	0.246	0.412	0.399	0.334	0.334	0.234
c_1	1.568	0.740	1.600	0.656	1.237	1.543	1.537	1.575	0.562	1.230
c_2	0.470	0.080	0.501	0.456	0.822	0.954	1.123	1.140	0.481	1.089
c_3	0.885	0.425	0.796	0	0	0	0	0	0	0

Table 7: Minimum form factor parameterization values.

	J/ψ	ψ'	$\psi(3770)$	$\psi(4040)$	$\psi(4160)$	$\psi(4415)$
M [GeV]	3.097	3.686	3.77	4.04	4.16	4.415
Γ_{ee} [keV]	5.26	2.14	0.26	0.75	0.77	0.47

Table 8: Masses and leptonic widths of the ψ-resonances (we take $\Gamma_{ee} = \Gamma_{\mu\mu}$).

As mentioned in section 4.2, the Breit-Wigner parameterization is a rather crude method for adding the resonances, moreover it results in double counting. As such, we have taken the difference between the results with and without the resonances included in C_9^{eff} at low s to be indicative of the maximal error introduced by adding the resonances, the true result lying somewhere in between. Thus both the results with and without this parameterization included will be shown in the figures below.

7.1.4 Wilson Coefficients in the Supergravity models

Two models of supergravity have been investigated (See section 6.2), differing only in the value of $\tan(\beta)$. In both cases, minimal as well as non-minimal scenarios have been included in the analysis. In all cases, the parameter spaces for C_7, C_9, and C_{10} have been calculated in [17]. Using these parameter spaces, we have investigated the coefficients with the combinations given in tables 9. The coefficients in the table should be taken as modifying the *pure* $C_{7,9}(m_b)$ parts of $C_{7,9}^{\text{eff}}$. The only experimental constraint we have included comes from measurements of the inclusive $B \to X_s\gamma$

decay from which the following constraint on C_7 arises [1]:

$$0.80 < |C_7/C_{7\mathrm{SM}}| < 1.20 \tag{79}$$

Note that the $\tan\beta = 30$ supergravity model allows C_7 to have the opposite sign of $C_{7\mathrm{SM}}$ and thus be positive. This results in higher branching ratios and a forward-backward asymmetry which has the opposite sign of the SM at low s (see fig.17).

Wilson coefficents in the supergravity models

	$C_7/C_{7\mathrm{SM}}$	$C_9/C_{9\mathrm{SM}}$	$C_{10}/C_{10\mathrm{SM}}$
	Supergravity $\tan\beta = 2$		
	0.800	1.015	0.990
	0.800	1.005	0.990
	0.800	1.005	0.970
I	**1.000**	**1.010**	**1.010**
	1.200	1.010	1.030
	1.200	1.000	0.920
II	**1.200**	**1.010**	**0.920**
	Minimal supergravity $\tan\beta = 2$		
	0.900	1.010	0.995
	0.900	1.000	0.995
	0.900	1.000	0.980
III	**1.000**	**1.010**	**1.010**
	1.200	1.010	0.995
IV	**1.000**	**1.005**	**0.980**
	1.200	1.010	0.980

	$C_7/C_{7\mathrm{SM}}$	$C_9/C_{9\mathrm{SM}}$	$C_{10}/C_{10\mathrm{SM}}$
	Supergravity $\tan\beta = 30$		
V	**-1.200**	**1.025**	**0.995**
	-1.200	1.025	0.955
	-1.200	1.000	0.995
	0.800	1.005	1.000
	0.800	0.995	1.000
VI	**0.800**	**0.995**	**0.980**
	1.200	1.000	1.000
VII	**1.200**	**1.000**	**0.995**
	Minimal supergravity $\tan\beta = 30$		
	-1.200	**1.010**	**0.990**
	-1.200	1.010	0.965
	-1.200	1.000	0.990
	0.800	1.0050	1.000
	0.800	1.000	1.000
	0.800	1.000	0.990
	1.200	**1.000**	**1.000**

Table 9: Allowed Wilson coefficient combinations for the minimal and non-minimal supergravity models. Boldface indicates the coefficients producing the maximal deviations from the SM in the branching ratios. These values, indicated by Roman numerals are the ones used in the plots below. In the non-minimal $\tan\beta = 30$ case, two minima have been chosen, as the $C_7/C_{7\mathrm{SM}} = 0.8$ case yields the smallest K^* branching ratio at small s whereas the $C_7/C_{7\mathrm{SM}} = 1.2$ case yields the lowest at high s (see fig.14).

Almost no difference was found between the results for the minimal and non-minimal $\tan\beta = 30$ models, thus only the non-minimal result will be shown in subsequent graphs. All results for the supergravity models have been calculated using the central values of the form factors (see table 5).

7.2 Decay distributions

Here, we present the branching ratios (both differential and integrated) for the decays $B \to K^{(*)}\mu^+\mu^-$, also valid for $B \to K^{(*)}e^+e^-$ due to the negligible mass difference. Thus μ can be exchanged for e everywhere in the following. The $\tan\beta = 2$ models are found to show rather small deviations from the SM result, moreover these deviations are swamped by the uncertainty in the form factors, the latter introducing uncertainties around (20-40)% in the decay distributions.

For the $\tan\beta = 30$ models, we find that the results for $B \to K^*\mu^+\mu^-$ can be changed by a factor of ≈ 2 by the $C_7/C_{7\mathrm{SM}} = -1.2$ model. This is more than the uncertainty produced by the form factors, making a direct experimental verification possible. For the decay $B \to K\mu^+\mu^-$, the maximal deviation is of the same order as the form factor related uncertainty, yet with maximal form factors, this result would still be distinguishable from the SM. With these results, we conclude that the branching ratio to K^* is the more well-suited for finding effects of supergravity.

In addition to the plots presented below for the differential branching ratios, we have calculated the total branching ratio by integration for both central, minimal and maximal values for the form factors. This integration has been performed on the differential distributions without the ψ resonances included. Note that these errors are theoretical errors, not statistical, thus all allowed values are equally probable with no special preference to the the central one.

Total Branching Ratios					
$B \to K\ell^+\ell^-$			$B \to K^*\ell^+\ell^-$		
	Model	$\mathrm{Br}_K/10^{-7}$		Model	$\mathrm{Br}_{K^*}/10^{-7}$
SM	standard model	$5.784^{+1.584}_{-0.865}$	**SM**	standard model	$19.59^{+5.01}_{-3.39}$
I	non-minimal $\tan\beta = 2$	$5.903^{+1.617}_{-0.882}$	**I**	non-minimal $\tan\beta = 2$	$19.98^{+5.11}_{-3.45}$
II	non-minimal $\tan\beta = 2$	$5.138^{+1.402}_{-0.764}$	**II**	non-minimal $\tan\beta = 2$	$17.83^{+4.58}_{-3.11}$
IV	minimal $\tan\beta = 2$	$5.684^{+1.556}_{-0.849}$	**IV**	minimal $\tan\beta = 2$	$19.23^{+4.92}_{-3.32}$
V	non-minimal $\tan\beta = 30$	$7.919^{+2.226}_{-1.225}$	**V**	non-minimal $\tan\beta = 30$	$36.94^{+10.2}_{-6.74}$
VI	non-minimal $\tan\beta = 30$	$5.787^{+1.588}_{-0.868}$	**VI**	non-minimal $\tan\beta = 30$	$19.35^{+4.93}_{-3.33}$
VII	non-minimal $\tan\beta = 30$	$5.600^{+1.530}_{-0.834}$	**VII**	non-minimal $\tan\beta = 30$	$19.44^{+5.01}_{-3.39}$

Table 10: Total Branching ratios for the decays $B \to K^{(*)}\ell^+\ell^-$ $(\ell = e, \mu)$ without the ψ resonances included. The roman numerals refer to the C_i in table 9. Note that **I=III**.

$\frac{dB(B \to K\ell^+\ell^-)}{ds}$ — Standard Model

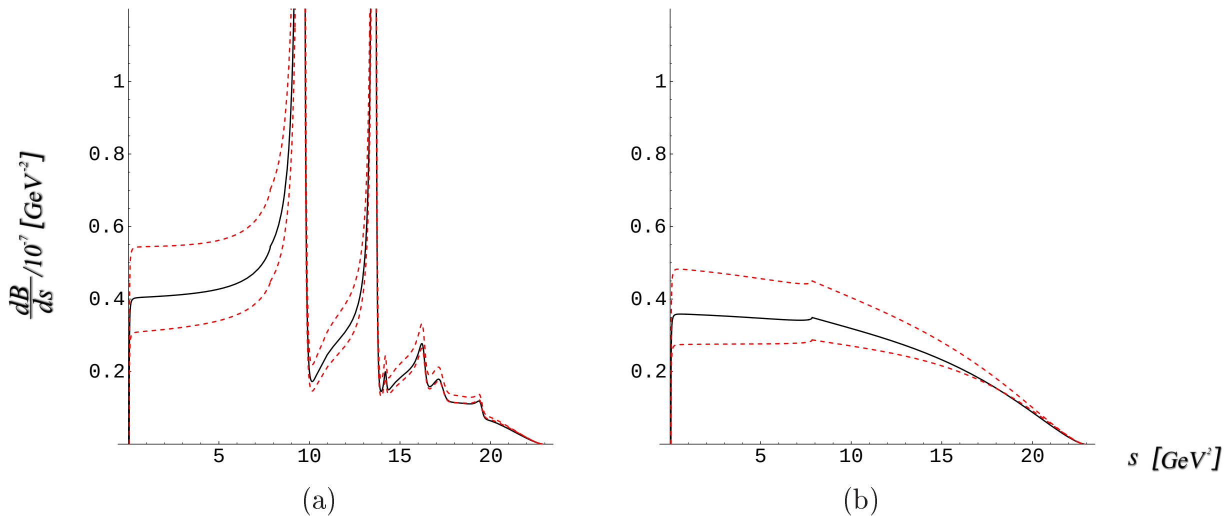

Figure 9: dB/ds for $B \to K\ell^+\ell^-$ ($\ell = e, \mu$) in the Standard Model (a) with the ψ resonances included in C_9^{eff} and (b) without. Theoretical errors arising from uncertainties in the form factors are shown with dashed lines.

$\frac{dB(B \to K\ell^+\ell^-)}{ds}$ — Supergravity $\tan\beta = 2$

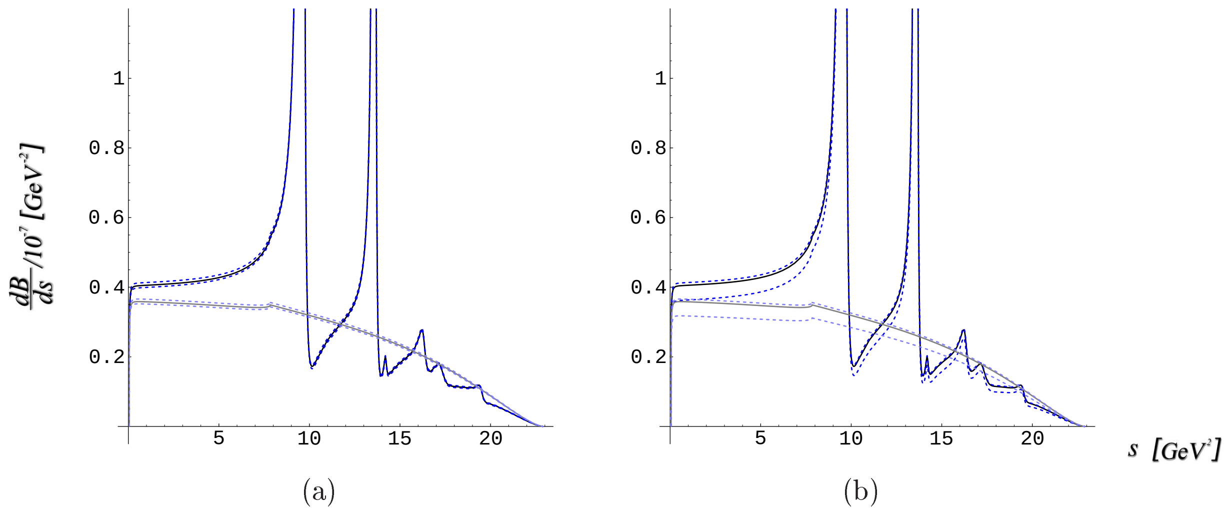

Figure 10: dB/ds for $B \to K\ell^+\ell^-$ ($\ell = e, \mu$) in (a) minimal and (b) non-minimal supergravity with $\tan\beta = 2$ (with and without the ψ resonances). For comparison, the SM predictions are shown as solid lines. The dashed curves represent maximal possible departure from the SM within the $\tan\beta = 2$ possibilities for C_7, C_9, and C_{10}. The fact that the largest deviation occurs to smaller values of the branching ratio in (b) comes from the fact that a very low C_{10} is possible in this model. This is, in fact, lower than the C_{10} possible in the $\tan\beta = 30$ models.

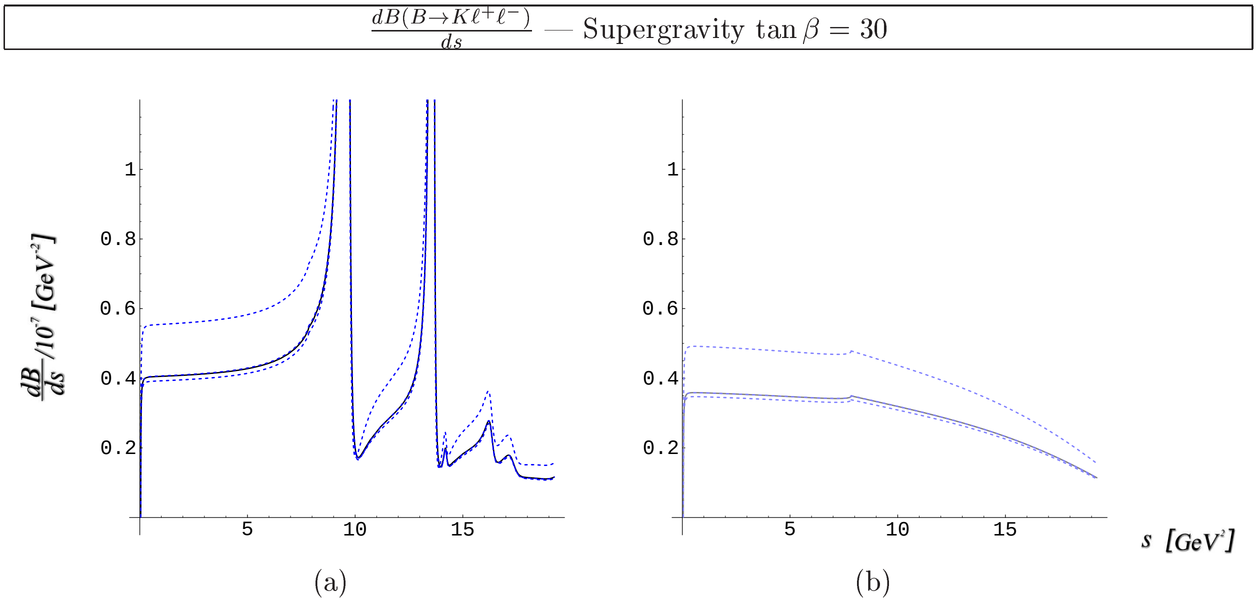

Figure 11: dB/ds for $B \to K\ell^+\ell^-$ ($\ell = e, \mu$) in non-minimal $\tan\beta = 30$ supergravity (a) with and (b) without the ψ resonances included in $C_9^{\rm eff}$. For comparison, the SM predictions are shown as solid lines. The dashed curves represent maximal possible departure from the SM within the $\tan\beta = 30$ parameter space for C_7, C_9, and C_{10}.

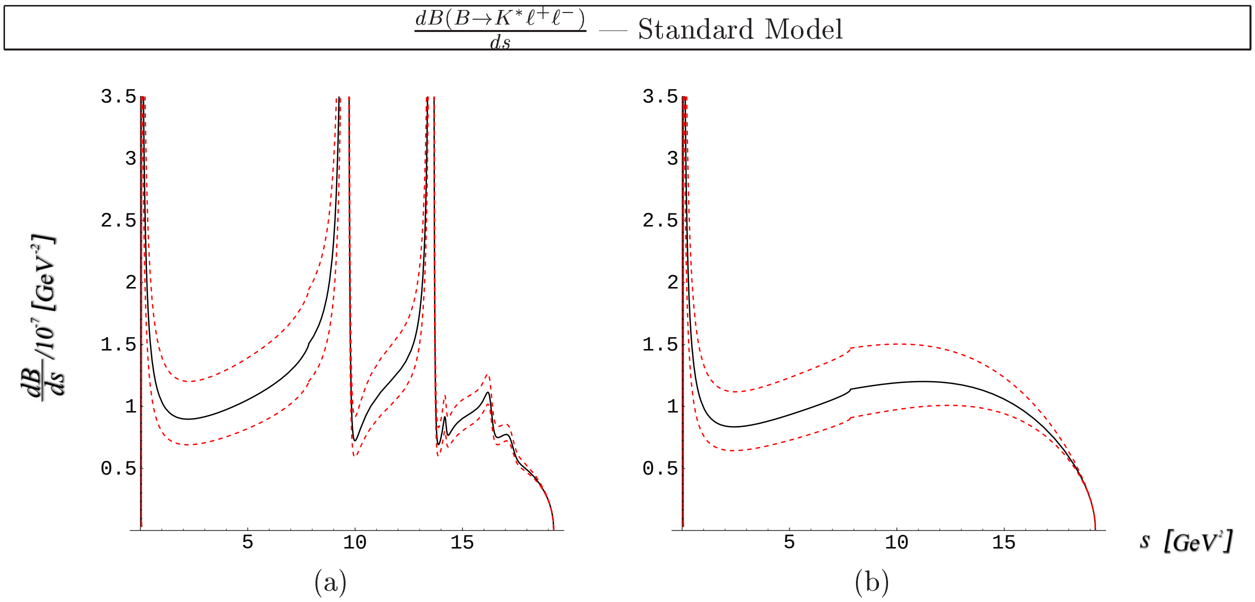

Figure 12: dB/ds for $B \to K^*\ell^+\ell^-$ ($\ell = e, \mu$) in the Standard Model (a) with the ψ resonances included in $C_9^{\rm eff}$ and (b) without. Theoretical errors arising from uncertainties in the form factors shown with dashed lines.

$\frac{dB(B\to K^*\ell^+\ell^-)}{ds}$ — Supergravity $\tan\beta = 2$

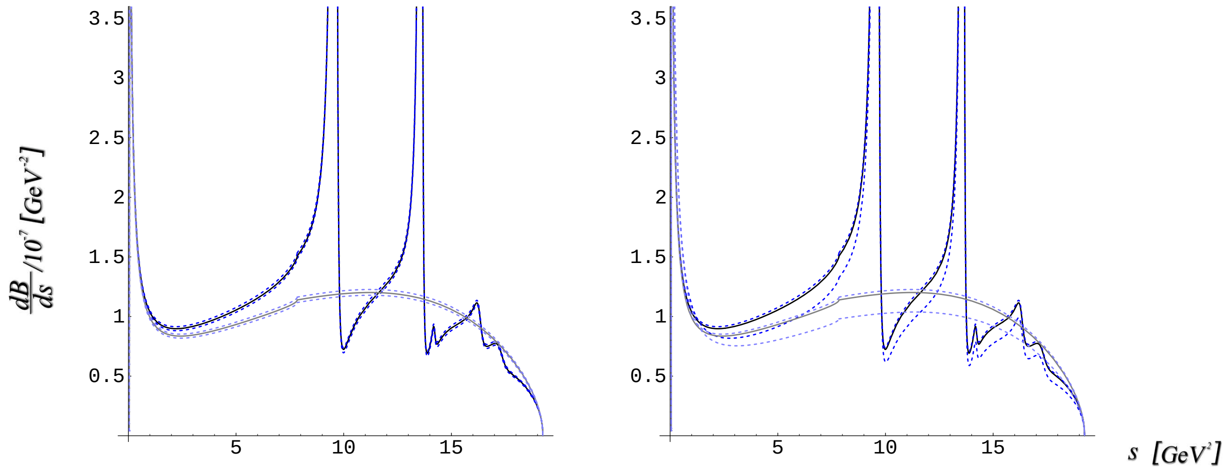

(a) (b)

Figure 13: dB/ds for $B \to K^*\ell^+\ell^-$ ($\ell = e, \mu$) in (a) minimal and (b) non-minimal supergravity with $\tan\beta = 2$. For comparison, the SM predictions (with and without the ψ resonances) are shown as solid lines. The dashed curves represent maximal possible departure from the SM within the $\tan\beta = 2$ parameter spaces for C_7, C_9, and C_{10}.

$\frac{dB(B\to K^*\ell^+\ell^-)}{ds}$ — Supergravity $\tan\beta = 30$

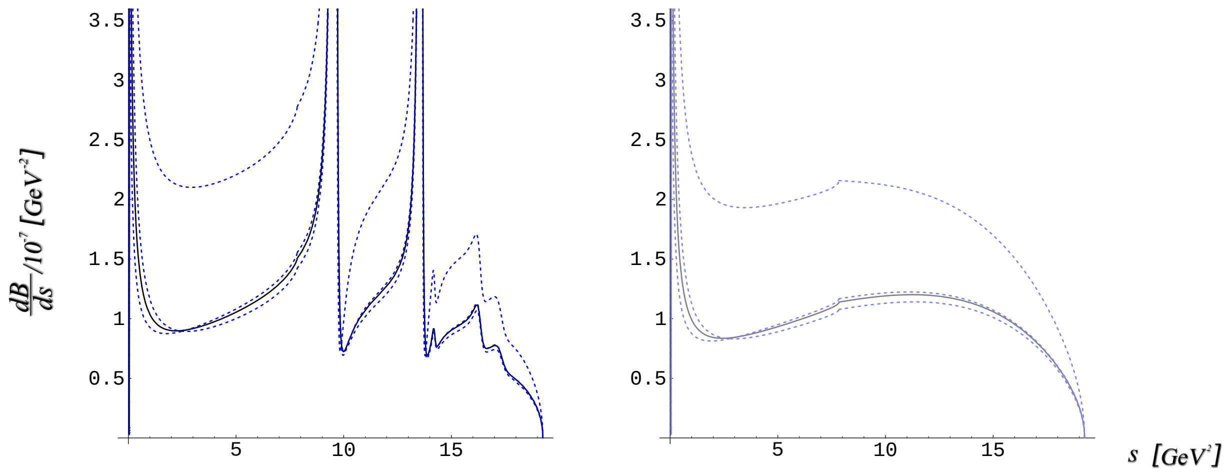

(a) (b)

Figure 14: dB/ds for $B \to K^*\ell^+\ell^-$ ($\ell = e, \mu$) in non-minimal $\tan\beta = 30$ supergravity (a) with and (b) without the ψ resonances included in $C_9^{\rm eff}$. For comparison, the SM predictions are shown as solid lines. The dashed curves represent maximal possible departure from the SM within the $\tan\beta = 30$ parameter space for C_7, C_9, and C_{10}.

7.3 Forward-backward asymmetries

As discussed in section 5.5, we here present results for the normalized FBA, i.e. the ratio of A_{FB} and the branching ratio.

We find that while the $\tan\beta = 2$ models hardly affect the results, the positive C_7 possible in the $\tan\beta = 30$ models produce a reversal of sign with respect to the SM at low s. This effect should be possible to measure experimentally in the near future (see the conclusion). Note, however, that $C_7 \approx C_{7\mathrm{SM}}$ is also possible in this model, thus a verification of the SM prediction is not in contradiction with $\tan\beta = 30$ supergravity (see section 6.3).

$\frac{d\bar{A}_{FB}}{ds}$ — Standard Model

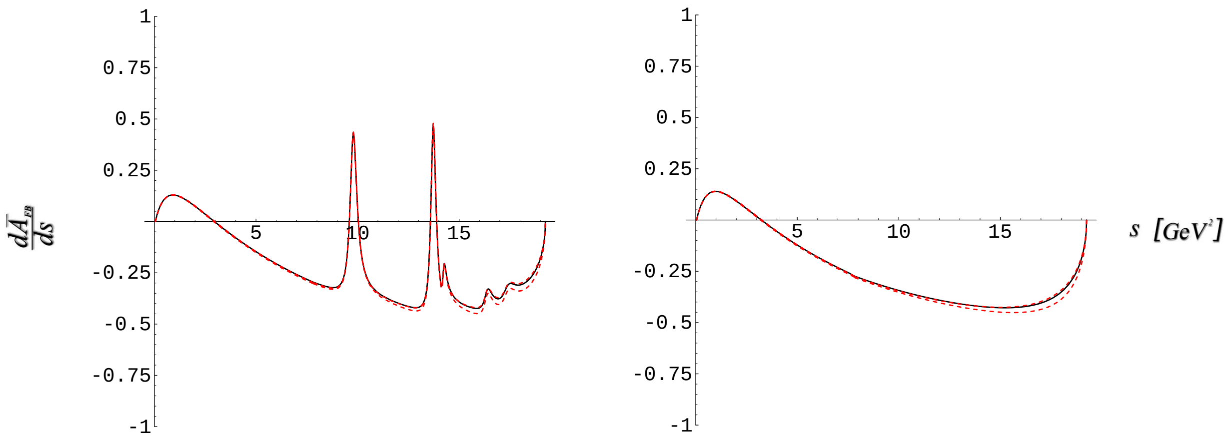

(a) (b)

Figure 15: Normalized Forward-Backward asymmetry, $\bar{A}_{FB}$, in the Standard Model (a) with the ψ resonances included in C_9^{eff} and (b) without. Theoretical errors arising from uncertainties in the form factors are shown with dashed lines. Note that the theoretical errors cancel to a large extent and are much smaller in the asymmetry than in the branching ratios.

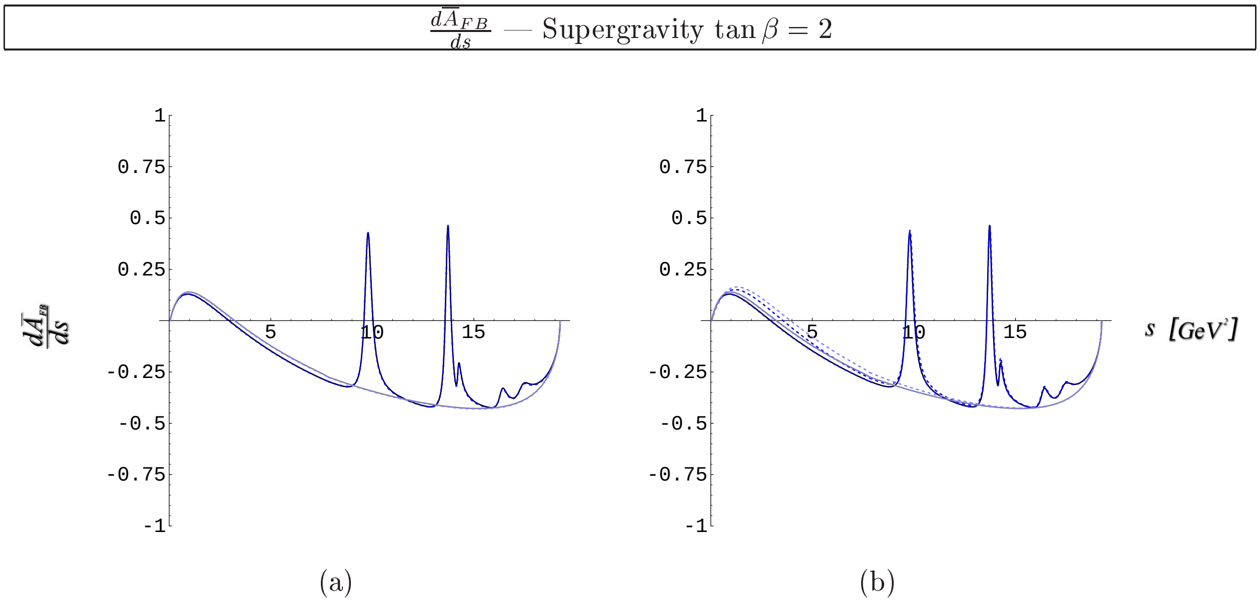

Figure 16: Normalized Forward-Backward asymmetry, $\bar{A}_{FB}$, in the (a) minimal and (b) non-minimal supergravity $\tan\beta = 2$ models. The dashed curves represent maximal possible departure from the Standard Model within the respective parameter spaces for C_7, C_9, and C_{10}.

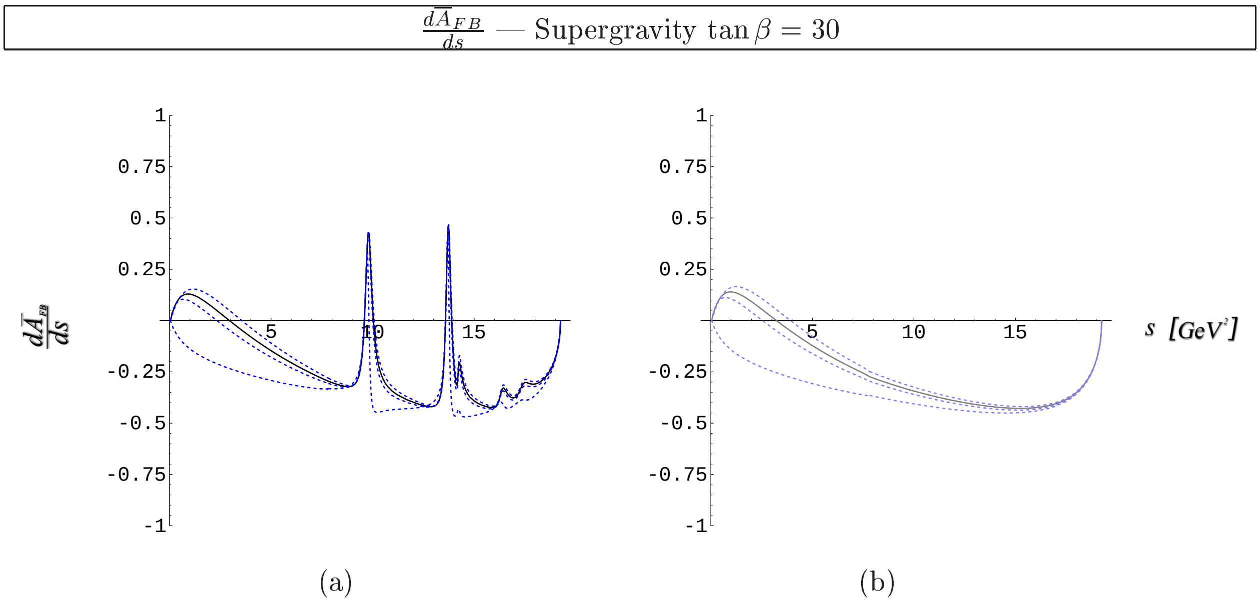

Figure 17: Normalized Forward-Backward asymmetry, $\bar{A}_{FB}$, in non-minimal $\tan\beta = 30$ supergravity (a) with and (b) without the BW fits included in C_9^{eff}. The dashed curves represent maximal possible departure from the Standard Model within the parameter space for C_7, C_9, and C_{10}. Note the change of sign at low s due to the positive $C_7 = -1.2 C_{7\text{SM}}$.

8 Concluding remarks

The basic phenomenology of FCNC transitions in Standard Model B physics has been reviewed, including discussions of GIM cancellation, Operator Product Expansion, and the Renormalization Group method, leading to a quark-level effective Hamiltonian describing the $b \to s\ell^+\ell^-$ decay at the scale m_b. From this Hamiltonian, a detailed analytical derivation of the matrix element for the decay $B \to K\ell^+\ell^-$ has been presented, neglecting the lepton masses, whilst the full calculation for both $B \to K\ell^+\ell^-$ and $B \to K^*\ell^+\ell^-$ has been performed using the `FORM` algebra engine. From these matrix elements, we have obtained expressions for the differential branching ratios and forward-backward asymmetries which have been implemented in `Mathematica` for numerical evaluation. A brief discussion of supersymmetry (supergravity) in the context of FCNC transitions has also been included, the effect of which is to alter the short-distance physics and thereby changing the decay distributions. A numerical analysis of these effects has been performed, enabling a direct comparison with the SM predictions.

The total branching ratios are found to be around 5×10^{-7} for the $B \to K\ell^+\ell^-$ decay and 2×10^{-6} for the $B \to K^*\ell^+\ell^-$ decay, depending on different scenarios of physics. The current limits originate from CDF and they are (90% confidence level) $\mathcal{B}(B \to K\ell^+\ell^-) < 5.2 \times 10^{-6}$ and $\mathcal{B}(B \to K^*\ell^+\ell^-) < 4.0 \times 10^{-6}$ [18], and thus experiments are just now reaching the limits for detection of these decays. Moreover, these decays will be studied at dedicated high-statistics machines such as BaBar, Belle, HERA-B, CDF and ultimately the LHC experiments ATLAS, CMS and LHC-b. BaBar and Belle expect to have on the low side of 10^8 $B\bar{B}$-decays, yielding around 25 $B \to K\ell^+\ell^-$ decays and 100 $B \to K^*\ell^+\ell^-$ decays with a low background, as they are e^+e^- colliders [4]. CDF and HERA-B[14] ($p\bar{p}$ colliders) expect to have a few more factors of statistics even though their efficiencies are low and backgrounds high. This increase in statistics should enable them to measure the sign of the forward-backward asymmetry at low s (see figure 17), thereby enabling a distinction between SM and $C_7 > 0$ supersymmetry. ATLAS, CMS and LHC-b will have at least an order of magnitude more data than all the other experiments, and the expectations for $B \to K^*\mu^+\mu-$ are around 5000 events [20], enabling a more refined distinction.

On the theoretical side, it is expected that the uncertainties on the form factors will reach the 10% level within the next few years [10], but unless some new development in solving QCD occurs, this error is hard to get further down, and thus we are faced with the perpetual problem of solving QCD. However, the high statistics at LHC will enable searches for other rare decays. The similar decay $b \to d\ell^+\ell^-$, which hadronically is $B \to (\rho, \pi)\ell^+\ell^-$, is suppressed by almost two orders of magnitude relative to $b \to s\ell^+\ell^-$ transitions[15], but holds equal if not even better opportunities for the study of rare decays. This will give new methods of searching for extensions of the SM, and so the game continues.

9 Acknowledgements

The authors would like to thank Prof. Alexander Khodjamirian not only for his supervision of this project, but for giving lectures in B-physics throughout the semester, which is the foundation of our knowledge on the subject. We would also like to thank Anders Wäänänen, Brian Aagaard Petersen and other members of the NBI-HEP group for enlightening discussions, in particular on supersymmetry. Finally we would like to thank NBI-HEP for providing office space, computer access and an inspiring and pleasant as well as scientific atmosphere.

[14] See [19] for HERA-B numbers.

[15] $\lambda^2 = 0.04$ in the Wolfenstein parameterization of the CKM matrix.

References

[1] A. Ali, P. Ball, L. T. Handoko and G. Hiller. A Comparative Study of the Decays $B \to (K, K^*)l^+l^-$ in Standard Model and Supersymmetric Theories. 1999. hep-ph/9910221.

[2] CLEO Collaboration. First Measurement of the Rate for the Inclusive Radiative Penguin Decay $b \to s\gamma$. *Phys. Rev. Lett.*, 10th April 1995.

[3] A. Vainshtein. How penguins started to fly - Sakurai prize lecture. 1999. hep-ph/9906263.

[4] C. Caso et al. Particle Data Group. Review of particle physics. *Eur. Phys. J. C 3*, 1998.

[5] A. J. Buras, R. Fleischer. Quark Mixing, CP Violation and Rare Decays After the Top Quark Discovery. 1997. hep-ph/9704376.

[6] T. Inami and C. S. Lim. Effects of Superheavy Quarks and Leptons in Low Energy Weak Processes. *Progr. Theor. Phys.*, 65:297, 1981.

[7] P. F. Harrison, H. R. Quinn, editors. *The BaBar Physics Book.* SLAC (R-504), October, 1998.

[8] A. J. Buras, M. Misiak, M. Münz, and S. Pokorski. Theoretical uncertainties and phenomenological aspets of $B \to X_s\gamma$ decay. 1993. hep-ph/9311345.

[9] T. Morozumi A. Ali, T. Mannel. Forward Backward Asymmetry of Dilepton angular distribution in the decay $b \to s\ell^+\ell^-$. *Phys. Rev. B273:505*, 1991.

[10] Alexander Khodjamirian. Private communication.

[11] F. Krüger and L. M. Sehgal. Lepton polarization in the decays $B \to X_s\mu^+\mu^-$ and $B \to X_s\tau^+\tau^-$. *Phys. Lett. B380:199*, 1996.

[12] A. Khodjamirian and R. Rückl. QCD sum rules for exclusive decays of heavy mesons. *Heavy Flavours II, ed. by A.J. Buras and M. Linder (World Scientific, Singapore)*, 1997.

[13] P. Ball and V. M. Braun. Exclusive semileptonic and rare decays in QCD. *Phys. Rev. D58:094016*, 1998.

[14] J. M. Flynn and C. T. Sachrajda. Heavy quark physics from lattice QCD. *Heavy Flavours II, ed. by A.J. Buras and M. Linder (World Scientific, Singapore)*, 1997.

[15] J. A. M. Vermaseren. *FORM manual.* 1989.

[16] A. Wiedemann H. J. W. Müller-Kirsten. *Supersymmetry. An introduction with conceptual and calculational details.* World Scientific, 1987.

[17] T. Goto, Y. Okada, and Y. Shimizu. Flavor changing neutral current processes in B and K decays in the supergravity model. 1998. hep-ph/9804294.

[18] CDF Collaboration (T. Affolder *et al.*). Search for the flavor changing neutral current decays $B^+ \to K^+\mu^+\mu^-$ and $B^0 \to K^{*0}\mu^+\mu^-$. *Preprint hep-ex/9905004*, 1999.

[19] Mogens Dam. Rare Decays at HERA-B. *Report from first working meeting, Dortmund, January 18th*, 1999.

[20] The LHC rare B-decay subgroup. Rare B-decays at LHC: Experiment. 1999.

A FORM-program

```
*----------------------------------------------------------------------
*                 B --> K* l- l+ decay distributions
*----------------------------------------------------------------------
Symbols A,B,C,D,E,F,G,H,mB,mKst,s,u,I;
Vectors pst,pB,pKst,q,r,eKst,p1,p2;
Indices mu,nu,al,al1,be,be1,mu1,nu1,rho,rho1;
*----------------------------------------------------------------------

Local L= 4*(p1(mu)*p2(mu1)-(p1.p2)*d_(mu,mu1)+ p1(mu1)*p2(mu));
Local L1=4*e_(p1,mu,p2,mu1);
id p1= 1/2*(q+r);
id p2= 1/2*(q-r);
id pst= pB+pKst;
id I*I  =-1;

Local M2BKstll=
(-d_(rho,rho1)+(pKst(rho)*pKst(rho1))/(mKst^2))*
((-I*A*e_(mu,rho,al,be)*pB(al)*pKst(be)-I*B*d_(mu,rho)+I*C*pB(rho)*pst(mu))*
(I*A*e_(mu1,rho1,al1,be1)*pB(al1)*pKst(be1)+I*B*d_(mu1,rho1)-I*C*pB(rho1)*pst(mu1))+
(-I*E*e_(mu,rho,al,be)*pB(al)*pKst(be)-I*F*d_(mu,rho)+I*G*pB(rho)*pst(mu))*
(-I*E*e_(mu1,rho1,al1,be1)*pB(al1)*pKst(be1)-I*F*d_(mu1,rho1)+I*G*pB(rho1)*pst(mu1)))*L
+
(-d_(rho,rho1)+(pKst(rho)*pKst(rho1))/(mKst^2))*
((-I*A*e_(mu,rho,al,be)*pB(al)*pKst(be)-I*B*d_(mu,rho)+I*C*pB(rho)*pst(mu))*
(-I*E*e_(mu1,rho1,al1,be1)*pB(al1)*pKst(be1)-I*F*d_(mu1,rho1)+I*G*pB(rho1)*pst(mu1))+
(-I*E*e_(mu,rho,al,be)*pB(al)*pKst(be)-I*F*d_(mu,rho)+I*G*pB(rho)*pst(mu))*
(-I*A*e_(mu1,rho1,al1,be1)*pB(al1)*pKst(be1)-I*B*d_(mu1,rho1)+I*C*pB(rho1)*pst(mu1)))*L1;

.sort
contract;

id pB.pB=mB^2;
id pKst.pKst=mKst^2;
id q.q  =s;
id r.r  =-s;
id r.q  =0;
* q.q = (pB-pKst)^2 = pB^2 + pKst^2 - 2pB.pKst ==> pB.pKst = 1/2(mB^2+mKst^2-s)
id pB.pKst=1/2*(mB^2+mKst^2-s);
* mKst^2 = (pB-q)^2 = pB^2 + q^2 - 2pB.q ==> pB.q = 1/2(mB^2-mKst^2+s)
id pB.q =1/2*(mB^2-mKst^2+s);
* u = 2pB.(p2-p1) = -2pB.r ==> pB.r = -u/2
id pB.r =-u/2;
* mB^2 = (pKst+q)^2 = pKst^2 + q^2 + 2pB.q ==> pKst.q = 1/2(mB^2-mKst^2-s)
id pKst.q =1/2*(mB^2-mKst^2-s);
* u = 2pB.(p2-p1) = -2pB.r ==> (pKst+q).r = -u/2 ==> pKst.r = -u/2
id pKst.r =-u/2;

.sort
contract;
bracket A,B,C,D,E,F,G,H;
print;
.end
```